Millimeter-wave Substrate Integrated Printed Ridge Gap Waveguide Leaky-Wave Antenna for WiGig Applications

Mohammad Reza Rahimi

A Thesis
In the Department
Of
Electrical and Computer Engineering

Presented in Partial Fulfillment of the Requirements
For the Degree of
Master of Science (Electrical and Computer Engineering) at
Concordia University
Montreal, Quebec, Canada

March 2018

CONCORDIA UNIVERSITY
SCHOOL OF GRADUATE STUDIES

This is to certify that the thesis prepared

By: Mohammad Reza Rahimi

Entitled: Millimeter-wave Substrate Integrated Printed Ridge Gap Waveguide Leaky-Wave Antenna for WiGig Applications

and submitted in partial fulfillment of the requirements for the degree of

Master of Science (Electrical & Computer Engineering)

Complies with the regulations of the University and meets the accepted standards with respect to originality and quality.

Signed by the final examining committee:

Dr. Chair

Dr.B.hamzeh External Examiner

Dr.John Zhangaurin Examiner

Dr.R.paknys Examiner

Dr.Shoukry Shams Examiner

Dr. A. Kishk Thesis Supervisor

Approved by: Dr. W. –P. Zhu, Graduate Program Director

April 3, 2018 Dr. A. Asif, Dean, Faculty of Engineering & Computer Science

Abstract

Millimeter-wave Substrate Integrated Printed Ridge Gap Waveguide Leaky-Wave Antenna for WiGig Applications

Mohammad Reza Rahimi, MASc.

Concordia University, 2018

Leaky-wave antennas have been an interesting topic for researchers for more than half a century. As millimeter-wave frequencies applications are in high demand for communication companies due their wider bandwidth, designing a leaky-wave antenna, for this frequency range is becoming more challenging with the demand for low-loss and low-cost components. Since high-performance hollow waveguides, as a low loss guiding structure, drives the cost to an unacceptable level and microstrip technology, as a low-cost transition, has an unacceptably high loss. Therefore, the requirements for a new technology that achieves both low cost and high performance feels more tangible.

The new technology of substrate integrated printed ridge gap waveguide that was proposed in 2016 shows promising characteristics as a new modified gap waveguide structure for millimeter-wave applications in terms of low insertion loss and low cost. Therefore, it is necessary to propose a new desirable class of microwave components based on this technology. Here, we propose the use of this technology to design three leaky-wave antennas.

The work of this thesis is divided into three major parts: (1) designing a periodic structure which has a leaky mode for a specific range of frequencies, and (2) designing a 1D-periodic leaky-wave antenna based on a periodic structure and connecting the antenna to the standard 50 Ω equipment. For achieving this purpose a quasi-TEM transition and a transition from microstrip to substrate integrated ridge gap waveguide has been designed. In addition, the slots of the proposed antenna are designed in order to have an almost constant leakage ratio through the whole operating frequency band. (3) The third part will discuss a linear array of the proposed antenna in which a new termination has been considered which results in a shorter physical length. The proposed antennas can be easily fabricated with a low-cost multi-layered PCB technology. In addition, all these antennas designed for the WiGig applications which are more attractive for today's requirements.

Keywords: Leaky-wave antenna; gap waveguide; electromagnetic band gap

Dedication

To Zahed and Mitra

Acknowledgments

I sincerely thank my supervisor, Prof. Ahmed Kishk for all his guidance and support. It was a real pleasure for me to have such an exceptional scholar and it was my honor to be his MASc student.

Furthermore, I would like to thank the committee members, Prof. Paknys, Prof.John Zhang, Dr. Shoukry Shamseldin, and Prof.Hamzeh for their review of my thesis and their numerous constructive comments and feedback.

Table of Contents

List of Figures

List of Tables

List of Acronyms

mm-wave	Millimeter-Wave
WLANs	Wireless Local Area Networks
WiGig	Wireless Gigabit
SIW	Substrate Integrated Waveguide
RGW	Ridge Gap Waveguide
CPW	Coplanar Waveguides
G-CPW	Grounded Coplanar Waveguides
VSWR	Voltage Standing Wave Ratio
TE	Transverse Electric Wave
TM	Transverse Magnetic Wave
TEM	Transverse Electromagnetic Wave
PMC	Perfect Magnetic Conductor

PEC	Perfect Electric Conductor
EBG	Electromagnetic Band Gap
AMC	Artificial Magnetic Conductors
CST	MWS Computer Simulation Technology Microwave Studio
PRGW	Printed Ridge Gap Waveguide
SIGW	Substrate Integrated Gap Waveguide
LWA	Leaky-Wave Antenna
1D-LWA	One Dimensional- Leaky-Wave Antenna
2D-LWA	Two Dimensional- Leaky-Wave Antenna
PLWA	Periodic Leaky-Wave Antenna
FWR	Fast Wave Region
SIGW-LWA	Substrate Integrated Gap Waveguide Leaky-Wave Antenna
MED-LWA	Magnetoelectric Dipole Leaky-Wave Antenna

Chapter 1

Introduction

1.1. Millimeter Wave Applications and Microwave Components

Today, millimeter-frequency bands are more attractive for mobile communications and for the future fifth-generation because of the high demands for high data rate. Wireless data rates in microwave frequencies and below are now limited to about 1 Gbit/s [1]. However, with the exponential increase of the number of users, this limitation is more tangible, and engineers are more eager to use millimeter frequencies for millimeter-wave components due to their higher bandwidth. Millimeter-wave (mm-wave) has the frequency range 30-300 GHz with the corresponding wavelength of 10 to 1 millimeter. In the mm-wave band, data rates can reach 10 Gbits/s and more [2]. However, the propagating signal suffers from attenuation due to the atmospheric absorption and cannot be used for long distance communications, but it is very attractive for short distance high-speed application. Typical applications included high-quality video transmission, which requires high data rate transfers. One of the most considerable frequency bands for high data rate wireless local area networks (WLANs) is 57 to 64 GHz band that can provide data rate up to 7 Gbits/s, which is called WiGig (Wireless Gigabit) [3]. There are a lot of considerable efforts to design microwave components for the WiGig application. Among the most common technology for microwave devices are the microstrip lines, substrate integrated waveguide (SIW) and hollow waveguide. The microstrip and SIW do not have acceptable performance at the mm-wave band due to the high insertion losses and dielectric losses. On the other hand, the hollow waveguide has a good performance in mm-wave frequencies, but the fabrication process is costly.

A new technology for guiding structure that can fill the gap between the performance of hollow waveguide and the low-cost of printed boards is the ridge gap waveguide (RGW). As compared to other waveguides, this type of waveguide has a higher quality factor and lower losses at mm-wave frequencies, which makes it a suitable choice. In addition, the printed version of a RGW with a lower bandgap is of low cost and easier to fabricate. Several mm-wave components have been designed based on the RGW and printed version of RGW illustrating

the promising capability of this technology for the millimeter-wave application in terms of cost-effectiveness and high-performance, which is desired for the today‘s requirements.

1.2. Microstrip, Coplanar Waveguides and Grounded Coplanar Waveguides

Microstrip, coplanar waveguides (CPW), and grounded coplanar waveguides (G-CPW) are kind of printed circuit guiding structures that have the capability to directly adapt to the antenna and microwave components [4], [5]. However, in the mm-wave bands, they suffer from significant losses due to the dielectric losses, conduction losses and radiation losses. In addition, using a thinner substrate requires using a narrower metal strip (usually matched to 50 Ω) that causes an increase of the conduction losses due to the high resistance. In addition, to the presence of discontinuities, we have surface waves which radiate, interfere, and cause coupling between multiple microstrip circuits. Figure 1-1 (a) shows the structure for a microstrip line. There is another type of guiding structures that can reduce the dielectric losses, which is referred to a suspended microstrip line. There is a gap between the substrate and ground in this structure. Figure1-1 (b) shows the structure of the suspended microstrip line. The fields contained in the air gap between the ground and substrate. However, if we increase the thickness of air gap, then the microstrip line will radiate.

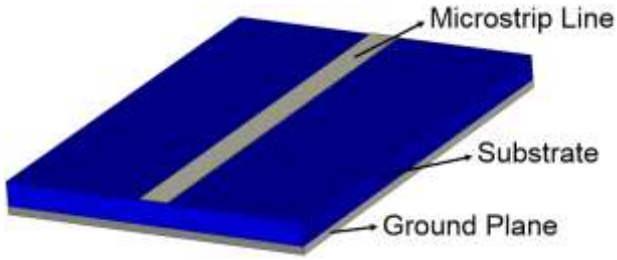

(a)

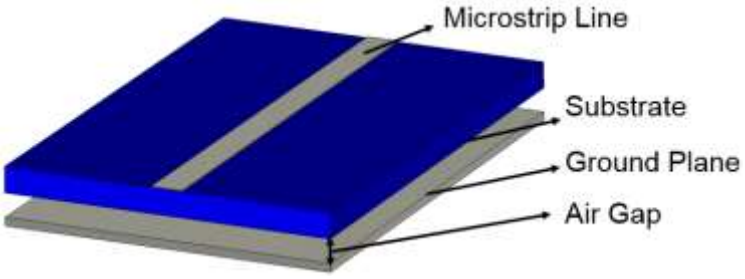

(b)

Figure1-1. (a) Microstrip line (b) Suspended microstrip line.

Another two guiding structures based on CPW and G-CPW, which are shown in Figure1-2 [6]. CPW consists of one separated central strip line and two ground planes, which are separated by two gaps. CPW is more flexible to design because of all conductors are in the same layer. However, they are suffering from dielectric losses. CPW excited unwanted modes due to the discontinuity such as T-junction. This disadvantage of CPW can be avoided by inserting air bridges over the center conductors to have the same potential on both ground planes and provide a shield over the discontinues parts. These air bridges can cause a lot of difficulty in the fabrication process and make it more complicated. On the other hand, the grounded CPW has less losses compared to the CPW. In grounded CPW a metallic plate is used under the substrate to provide isolation from other circuits in the lower layers. Proper grounding is achieved by using via holes between the ground plane and the bottom shield. In addition, tuning the impedance of the grounded CPW is easily achieved by changing the space between the grounds and the signal line. The disadvantage of the grounded CPW is its suffering from losses in the mm-wave frequency range, which makes it less efficient for these ranges of frequencies.

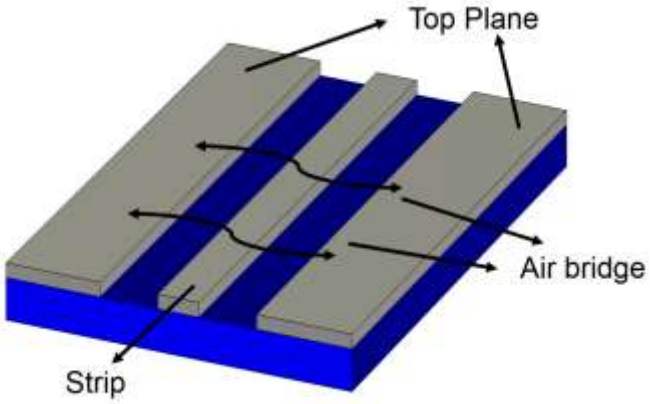

(a)

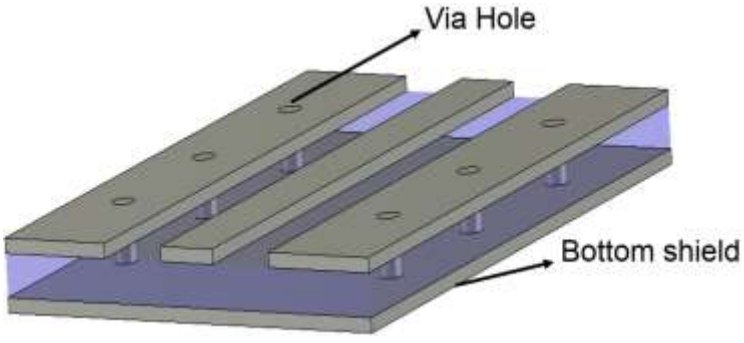

(b)

Figure1-2. (a) Coplanar waveguide (b) Grounded coplanar waveguide.

1.3. Hollow Waveguides and Substrate Integrated Waveguides

Another kind of guiding metallic structure is the hollow waveguide. Figure1-3 shows the structure of hollow waveguide. The hollow waveguide in comparison with the microstrip transmission line has a lot of advantages. For instance, they have high power handling capability, their insertion loss is low because of high Q factor [7], the Voltage Standing Wave Ratio (VSWR) is close to 1, and the shielding effectiveness is very high [8] compared to the other waveguides. The hollow rectangular waveguide can propagate TM (transverse magnetic) and TE (transverse electric) modes, but not TEM (transverse electromagnetic). The dominant mode of the rectangular waveguide is TE_{10} because it has the lowest cutoff frequency. There is a difficulty in matching this waveguide because of their rigid, hollow-pipe shape. Special couplings at the joints are required to assure proper operation. For decreasing the skin effect losses, the inside surfaces of the waveguide are plated with silver or copper. In addition, the width of this waveguide must be the half wavelength of the operating frequency. Therefore, the waveguide is increasingly impractical for frequencies below 1 GHz. In addition, at the mm-wave frequencies, the wavelength becomes very small, and the realization with current matching is very complicated and challenging. Moreover, manufacturing tolerances are a crucial problem at mm-wave frequencies, which can affect the performance of the hollow waveguide. All the above requirements increase the cost and make the fabrication more complicated for this kind of waveguide.

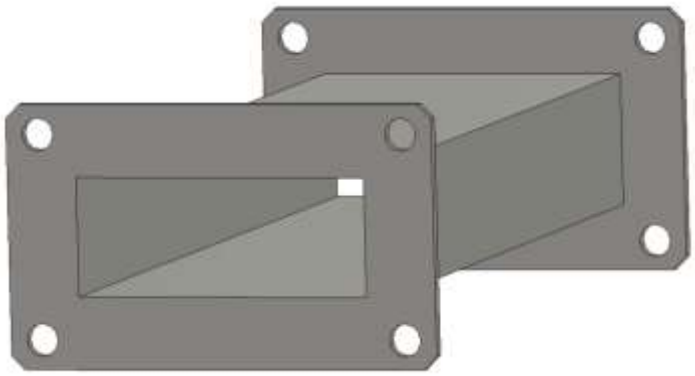

Figure1-3. Hollow rectangular waveguide.

The dielectric-filled waveguide is another type of waveguide, which is referred to substrate integrated waveguide (SIW), which was introduced in [9] and [10]. This waveguide has less weight and is lower cost compared to the hollow waveguide. SIW has a high-quality factor, and their insertion losses are usually less than 0.4dB/m (lower than a microstrip line) in the Ka-band [11]. This planar waveguide is realized in the printed circuit technology. The geometry of SIW is shown in Figure1-4. The via diameters and the distance between them play a significant role in controlling the leakage in SIW structure. According to [12], to decrease the leakage, there are two points that must be considered in the design of SIW structures. First, the diameter of the via (d) must be less than λ_g / 5. Secondly, the periodicity of the vias (P) should be p < 2d. The field is traveling in the substrate between the two rows of vias hole. This via hole act as the metal side walls of the hollow waveguide. Therefore, the SIW presents similar dispersion characteristics as the standard waveguides. However, because of using the dielectric material in SIW structures, these structures suffer from high dielectric losses in mm-wave frequencies. In addition, they are suffering from radiation losses due to the vias holes, which do not provide a perfect metal shield [13].

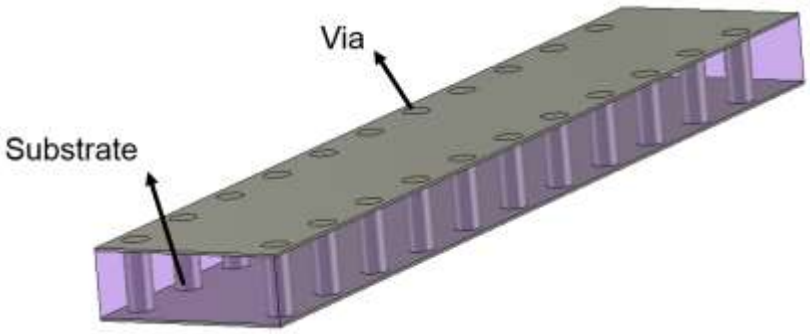

(a)

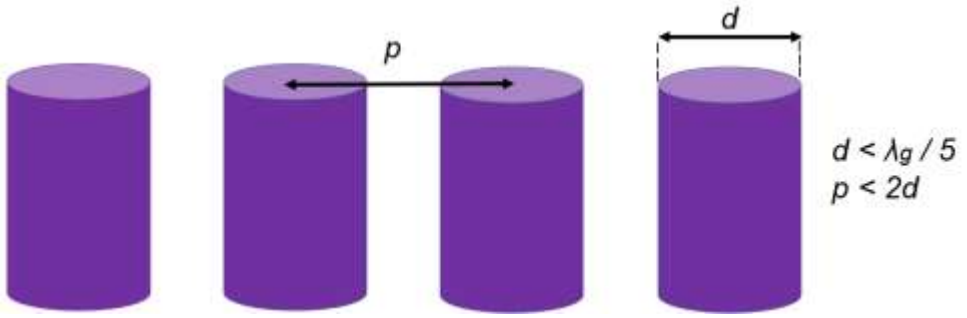

(b)

Figure1-4.(a) Substrate integrated waveguides and (b) The vias dimension and periodicity condition.

1.4. Soft and Hard Surfaces

Soft and hard surface structures were introduced by Kildal in 1988 [14]. The basic idea of soft and hard surfaces is related to controlling the propagation of the electromagnetic waves along the corrugated surfaces. Generally, a soft surface stops the waves from propagation, whereas a hard surface allows the wave to propagate along the corrugation. A typical soft surface is realized by transverse corrugations as shown in Figure1-5 (a) where the depth of the corrugation, d, is a quarter wavelength, the short circuit is transformed to an open circuit at the top of the corrugation, and the surface impedance will be infinite along the direction of propagation. Therefore, for narrow, smooth corrugation, there is approximately no electromagnetic wave propagation. By the other term, the power flux density at the surface is equal to zero. This means that this structure can suppress the transverse electric field and transverse magnetic field along the surface. Therefore, the waves will be stopped from propagation. Soft surfaces are used in many applications such as corrugated horn antennas as feeds for reflector antennas [15], [16]. It can be used as isolation between the aperture of the horn and the feeding network, in addition, it can improve the back-lobe radiation of the horn antenna. On the other hand, hard surfaces can eliminate only the longitudinal field components, and this structure supports the propagation of the only TEM mode. The corrugation of the hard surface can be realized by metal strips over grounded dielectric substrate or dielectric filled corrugated grooves. The grooves and the dielectric thickness are quarter guiding wavelength depth. The dielectric material should have a dielectric constant higher than the permittivity of the medium above the surface as shown in Figure1-5 (b) with the depth:

$$d = \lambda / (4\sqrt{\varepsilon r - 1}) \quad (1.1)$$

Hard surfaces can be used in many applications. We usually use hard surfaces when we need strong propagation on the surface. It is mostly applied to the concept of the hard waveguide in which quasi-TEM modes can propagate along the longitudinally dielectric filled corrugation. This structure is usually used in horn antenna for increasing the aperture efficiency [17]. In addition, hard surfaces can be used in miniaturized array elements for multi-frequency applications [18]. However, the disadvantage of hard surfaces is their losses and narrow band.

Periodic strips of PMC/PEC strips can model soft and hard surfaces as shown in Figure 1-6(a). When the strips are longitudinal, the electromagnetic wave can propagate, and it acts as hard surface, and for transverse strips, it acts as soft surfaces, and it stops the electromagnetic wave from propagation. In [19], it was demonstrated that local quasi-TEM modes could propagate along the ridges of corrugation when we have a metal plate on the top of the corrugation surfaces, at a distance less than a quarter wavelength as shown in Figure1-6 (b). The operating principle of this structure is the same as PEC/PMC strips with a metal plate on top. The wave is profoundly attenuated after crossing a few of these PEC/PMC strips in the transverse direction due to the anisotropic characteristic of the PEC/PMC strips. Therefore, the electromagnetic waves propagate only in the longitudinal direction as shown in Figure1-7. The concept of soft and hard surfaces explains a 1D periodic structure where the PEC/PMC strips are repeated in one direction. There are other periodic structures that implement the periodicity in two dimensions. These structures called Electromagnetic Band Gap (EBG) structures. A brief discussion about the EBG structures will be addressed in the following section. This concept has been improved in [20] to introduce a new type of waveguide, which is referred to a gap waveguide. The gap waveguide can be defined as a new type of hard waveguide with the advantage of being a wideband and low loss (high Q factor) for mm-wave frequencies compared to the hard waveguides [21].

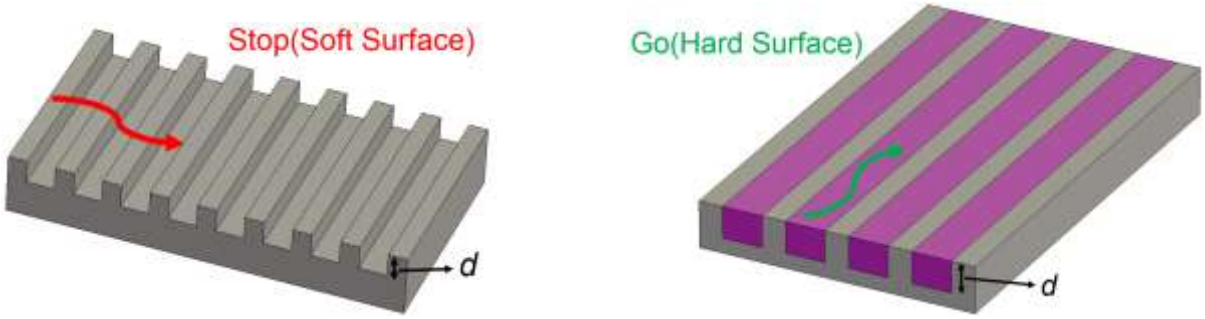

(a) (b)

Figure1-5. (a) Soft surface realized with transverse corrugations. (b) Hard surface realized with longitudinal dielectric filled corrugations.

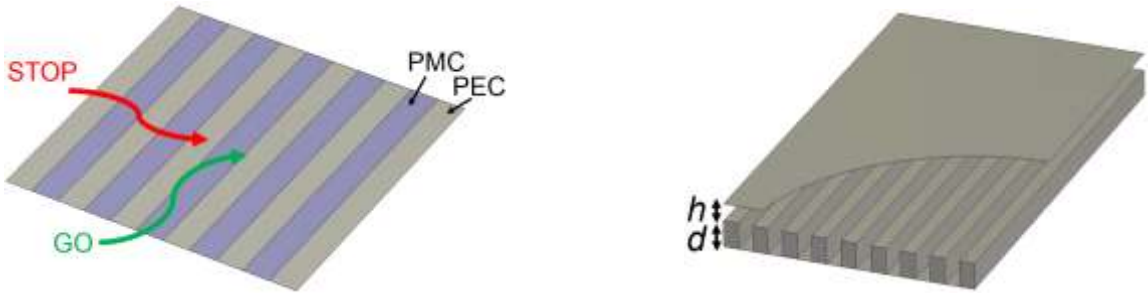

(a) (b)

Figure1-6. (a) Soft-Hard surface ideally realized with PEC/PMC strips. (b) Single hard wall waveguide.

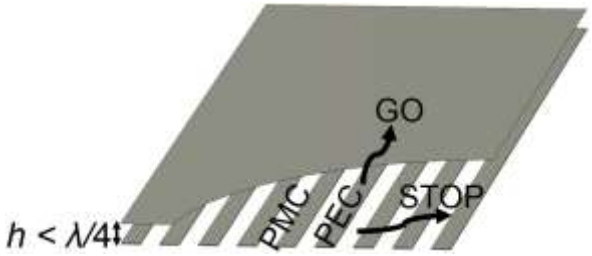

Figure1-7. Ideal PEC/PMC interpretation of the corrugated surface and its overall effect on the waves.

1.5. Gap Waveguide Technology

In the last few years, there has been a lot of research on the gap waveguide guiding structures [22], [23], and [24]. Gap waveguide technology is a recently developed technology for the soft and hard surfaces. Gap waveguide uses the basic cutoff of a PEC-PMC parallel plate waveguide configuration to control the wave propagation between the two parallel plates. If the distance between the top metal plate and the PMC surface is less than λ/4, then no waves can propagate in any direction between the two surfaces. However, if we put a metal strip on the PMC surface, then the wave can propagate only along the metal strip, and waves in other directions are evanescent when h < λ/4 for the vertical polarization (TM_n case) and when h is λ/2 for the horizontal polarization (TE_n case). Thus, the proper gap must be less than λ/4 [20]. PMC has no exist in nature. Therefore, we must artificially realize it. Then, they are usually referred to as artificial magnetic conductor (AMC) due to the boundary condition that they provide, which is the tangential of the magnetic field is zero at the surface. Figure1-8 shows the basic concepts for the gap waveguide technology.

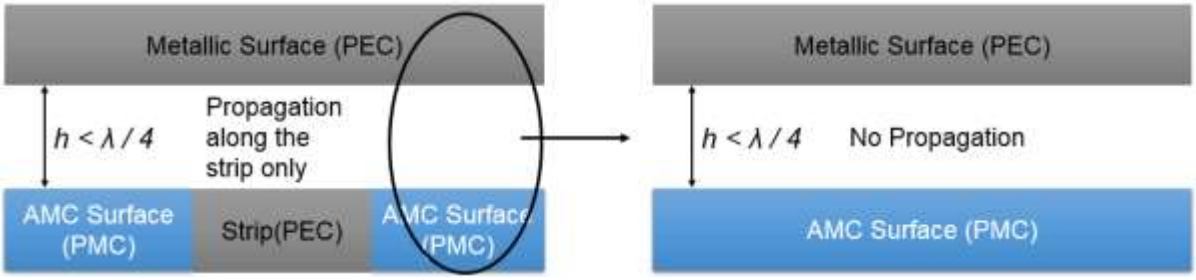

Figure1-8. Gap waveguide cross section.

One of the advantages of the gap waveguide is that there is no connection between the upper and lower metallic surface, which makes them a suitable choice with low cost and low loss waveguides component, especially for millimeter wave frequency bands. This concept can be realized with different technologies. For example, microstrip gap lines [25], ridge gap waveguide [26] and groove gap waveguides [27]. The two first waveguides support quasi-TEM mode, and groove gap waveguide supports TE_{10} mode. It should be noted that the characteristic impedance of the quasi-TEM line varies with the frequency [28]. Groove gap waveguide has fewer losses (higher Q factor) compared to the RGW losses due to the more volume of the current density. However, the resonant length of them can be affected by the tolerance on the position of pin walls compared to the rectangular waveguide that has larger Q_s. In order to have more flexibility in the design, microstrip gap waveguide was introduced in [29]. In this kind of waveguide, the dielectric losses are not severe compared to the conduction losses. Figure1-9 shows these three gap waveguide configurations. There is also some new modified version of gap waveguide, which will be explained in the following sections.

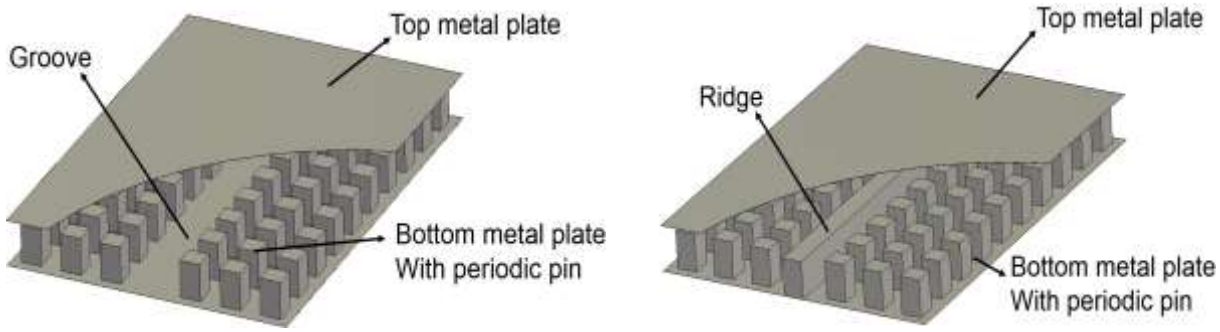

(a) (b)

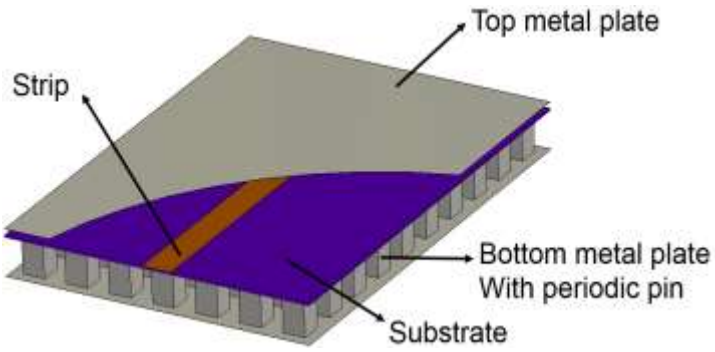

(c)

Figure1-9. Three different gap waveguide: (a) Groove gap waveguide, (b) Ridge gap waveguide, and (c) Microstrip gap waveguide.

1.6. Ridge Gap Waveguide Technology

Ridge gap waveguide (RGW) is introduced in [30] as a new type of waveguide structure for the millimeter-wave application, which is realized with two parallel metallic plates with a central metal ridge, which is surrounded by the periodic pins. RGW structure has the ability to create a Band Gap for wave propagation in the undesired direction. This band gap is achieved by using a periodic structure of pins near the guiding ridge of RGW. These periodic nails referred to as a bed of nails in [28]. The bed of nails can act as high impedance surface only with the condition that the height of the air gap is less than $\lambda/4$. The periodic EBG structure should be designed to cover a specific frequency band. This Band Gap is related to the geometry parameters of the bed of the nail unit cell. A detailed study to investigate these effects can be found in [31]. Moreover, the existence of the ridge has a significant effect on the bandwidth [31] Figure 1-10 (a) shows the structure dispersion diagram of a unit cell of RGW. The dispersion diagram has been calculated with MWS Computer Simulation Technology Microwave Studio (CST) Eigenmode solver. The band gap of the unit cell is from 64.45 to 96.46 GHz.

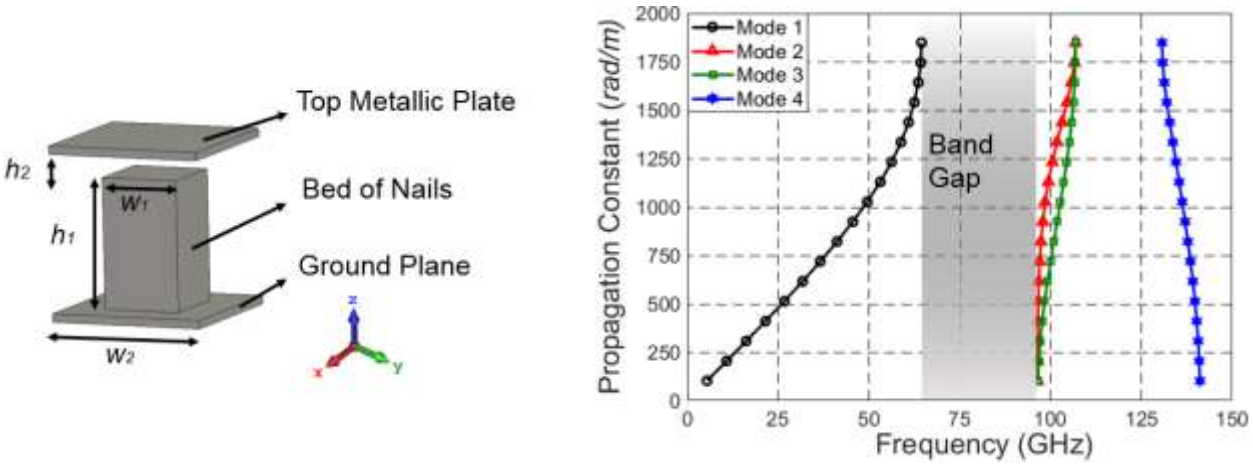

(a) (b)

Figure 1-10. (a) Unit cell dimensions (h_1 = 0.765 mm, h_2 = 0.254 mm, w_1 =1.7 mm, w_2 = 1.3 mm). (b) Dispersion diagram of a periodic bed of nail structure as an EBG unit cell.

A single row of the RGW is shown in Figure 1-11 (a).The width of the ridge is tuned to match with 50 Ω. Three unit cells are enough to suppress the leakage around the ridgeline. To calculate the characteristic impedance of the transition line different approach can be taken. A closed-form equation introduced in [28], which has good agreement with the CST results. The dispersion diagram of a single row of the RGW is shown in Figure 1-11 (b). The band gap for the single row of RGW is smaller than the band gap of RGW unit cells, which is from 64.8 GHz to 90.8 GHz.

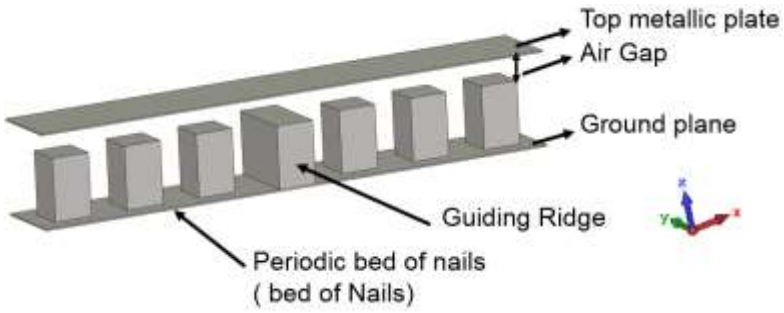

(a)

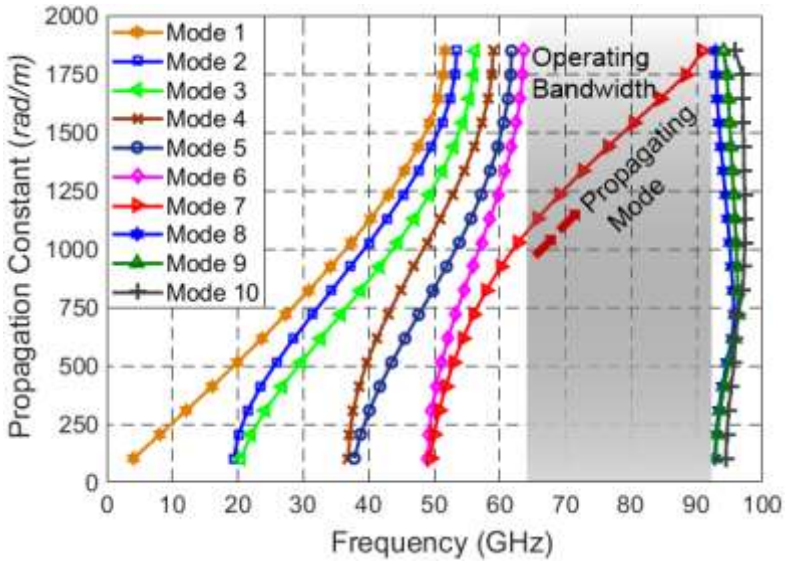

(b)

Figure1-11 (a) Configuration of a single row of RGW. (b) Dispersion diagram of RGW that consist of semi-periodic fakir nails and a guiding ridge.

1.7. Printed Ridge Gap Waveguide

There is another type of RGW that was introduced in [32], which is called printed ridge gap waveguide (PRGW). The geometry of PRGW unit cell is shown in Figure 1-12 (a). The unit cell has a rectangular patch grounded by a plated via including one substrate with an air gap between the substrate and upper metallic plate. The performance of PRGW regarding the loss is much better than the conventional microstrip waveguide. In addition, compared to the RGW, manufacturing cost of PCB fabrication is significantly lower than CNC machining. The dispersion diagram of the PRGW unit cell is shown in Figure 1-12 (b), which shows the band gap of the unit cell is 45.8-82.6 GHz. A single row of the PRGW is shown in Figure 1-13. Similar to the RGW, three unit cells are sufficient to suppress the leakage around the ridgeline. In order to suppress any of the possible propagating modes under the continuous printed ridge and to realize as a ridge, a single row of metallic vias is placed under the guiding ridge connecting it to the ground (according to the structure, the number and location of the vias could be changed). The width of the ridge is tuned to match with 50 Ω as in Figure 1-13. The dispersion diagram of a single row of PRGW in Figure 1-14 shows that the band gap is little less than the unit cell band gap, which is 46.02-80.7 GHz.

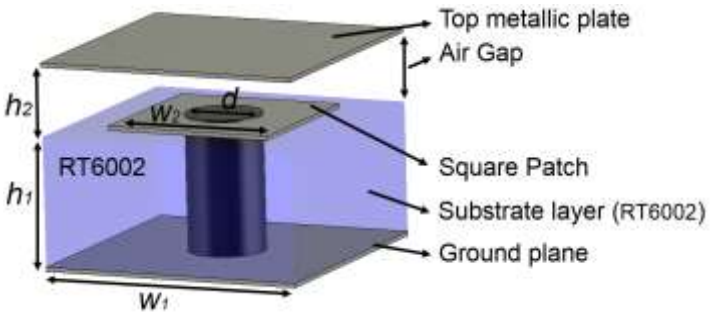

(a)

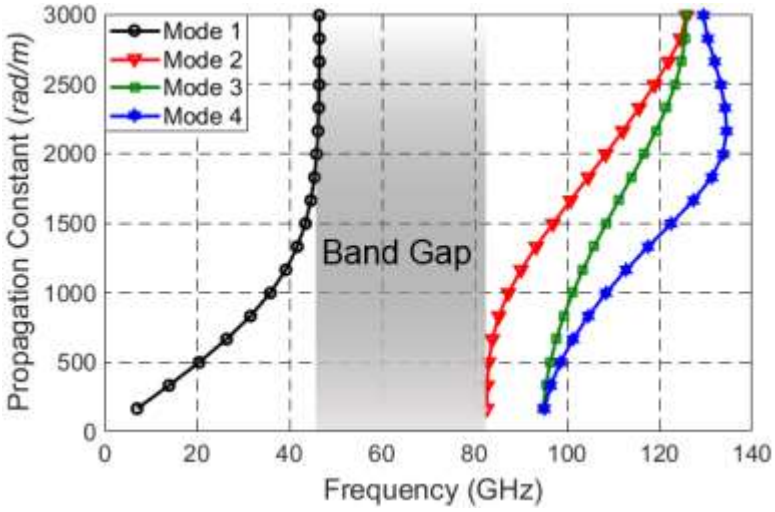

(b)

Figure 1-12. (a). Unit cell dimensions (h_1 = 0.508 mm, h_2 = 0.254 mm, w_1 =1.05 mm, w_2 = 0.67 mm). (b). Dispersion diagram of a plated via topped by a square patch.

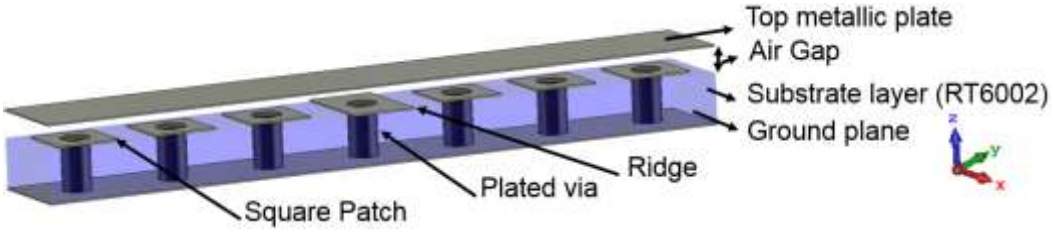

Figure 13. Configuration of a single row of PRGW (one substrate layer with an air gap).

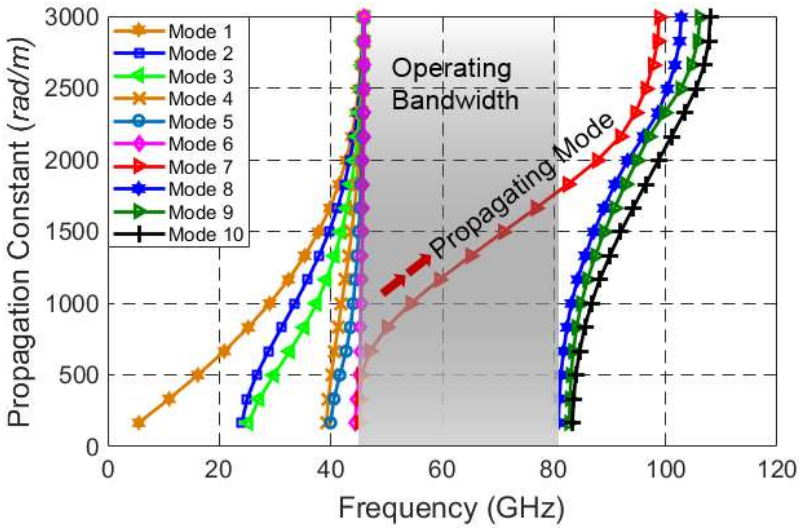

Figure1-14. Dispersion diagram of a PRGW consists of semi-periodic plated vias and short-circuited ridge.

1.8. Substrate Integrated Printed Ridge Gap Waveguide

As ensuring the thin air gap height for PRGW structures at millimeter waves is becoming a problem for large structures, the gap is filled with thin low loss and low dielectric constant substrate layer to guarantee a fixed gap height between the PEC and AMC layers over the structure. Therefore, a modified version of PRGW called as substrate integrated gap waveguide (SIGW) was introduced in [33], in which a low loss thin substrate is filling the gap to fix the gap height over the circuit. This technology used in [34] to increase the aperture of a horn antenna and the operational bandwidth. SIGW technology as compared to the RGW technology has lower cost, and the fabrication process is much easier. The geometry of SIGW unit cell is shown in Figure 1-15 (a). The unit cell has a rectangular patch grounded by a plated via including two substrates. The dispersion diagram of the proposed unit cell is shown in Figure 1.15 (b), which shows the band gap to be 41.5-82.8 GHz. A single row of the SIGW is shown in Figure 1-16. The condition of the vias and mushrooms are same as the condition of PRGW. The width of the ridge is tuned to match with 50 Ω in Figure 1-16. The dispersion diagram of the single row of SIGW shown in Figure 1-17 is little less than the unit cell bandgap, which is 41.8-80.2 GHz.

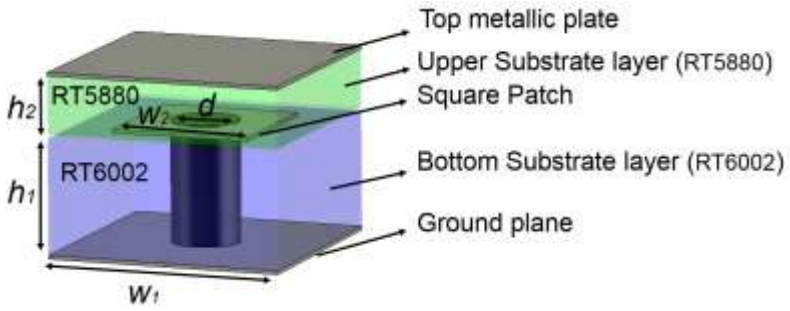

(a)

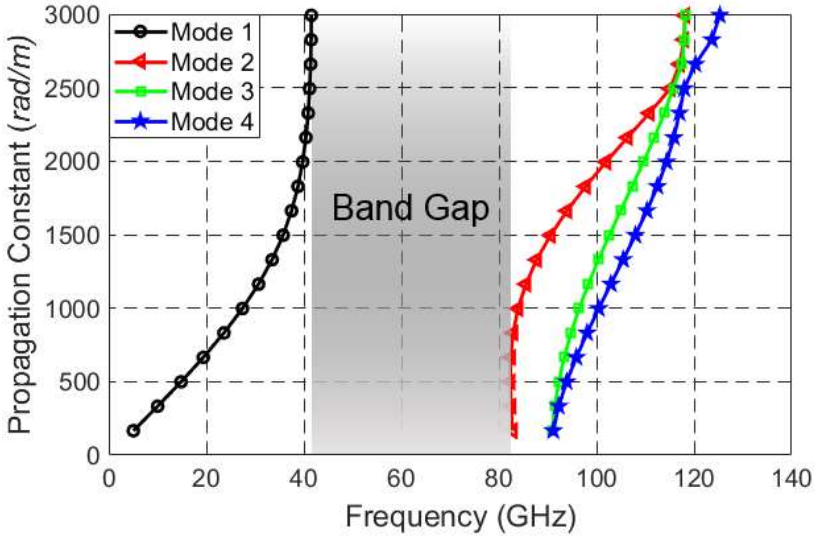

(b)

Figure 1-15. (a). Unit cell dimensions (h_1 = 0.508 mm, h_2 = 0.254 mm, w_1 =1.05 mm, w_2 = 0.67 mm). (b). Dispersion diagram of a plated via topped by a square patch.

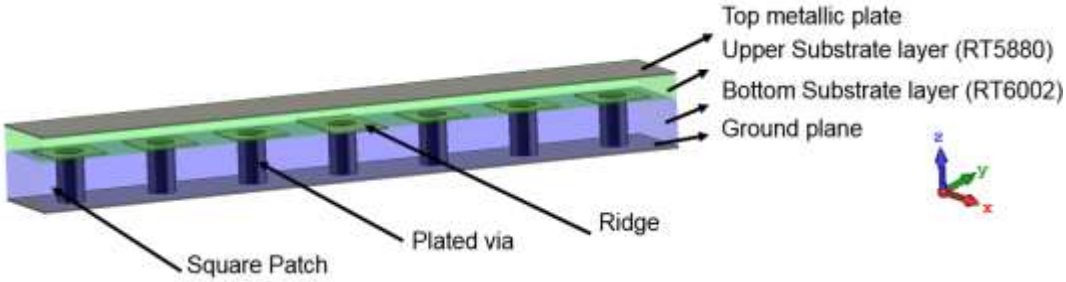

Figure1-16. Configuration of a single row of SIGW consists of two layers of the substrates.

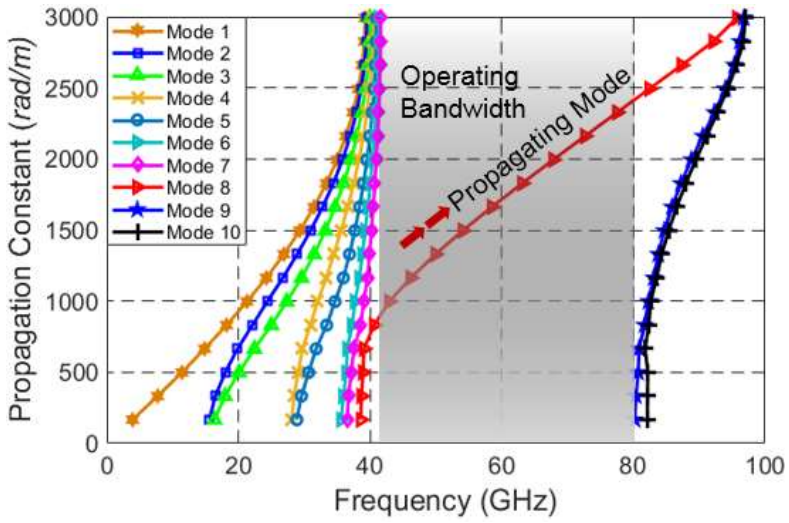

Figure1-17. Dispersion diagram of a SIGW consists of semi-periodic plated vias and short-circuited ridge.

There is another modified version of SIGW introduced in [35]. The unit cell structure is similar to the SIGW unit cell, but there is an air gap between the second layer of the substrate and the top metal plate resulting in a low-loss planar circuit using SIGW. In addition, the design process is simplified regarding the placement of the cells around the resonators and lines. The structure and dispersion diagram of the modified SIGW are shown in Figures 1-18 and 1-19, which show that the unit cell has the band gap of 22.4-44.6 GHz. A single row of the modified SIGW is shown in Figure 1-20. The condition for the mushroom and via is similar to the SIGW and PRGW. The width of the line is tuned to match 50 Ω, Figure 1-20 (a). The dispersion diagram of the single row of SIGW shown in Figure 1-20 (b) is little less than the unit cell bandgap, which is 41.8-80.2 GHz.

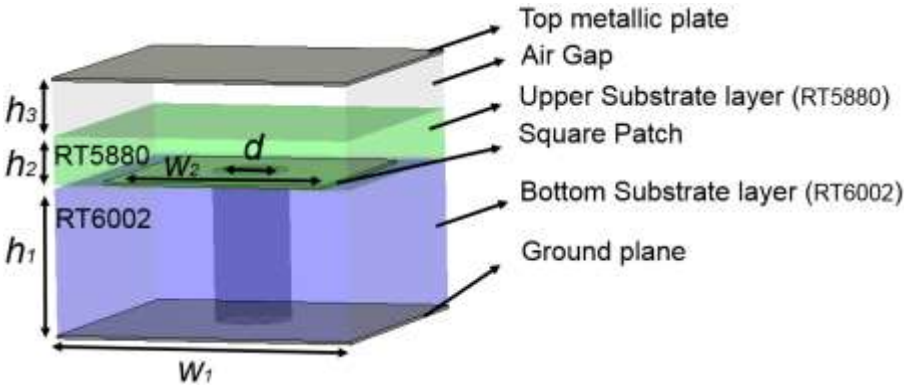

Figure1-18. Configuration of a single cell of SIGW consists of two layers of substrate and air gap (h_1 = 0.765 mm, h_2 = 0.254 mm, h_3 = 0.288 mm, w_1 =1.6 mm, w_2 = 1.2 mm, d =0.4 mm).

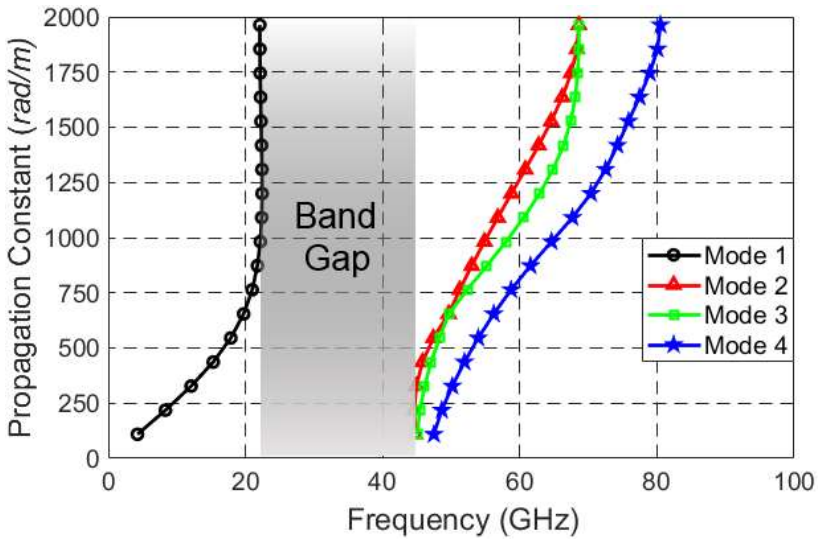

Figure1-19. Dispersion diagram of modified SIGW unit cell with two-layer substrates and air gap.

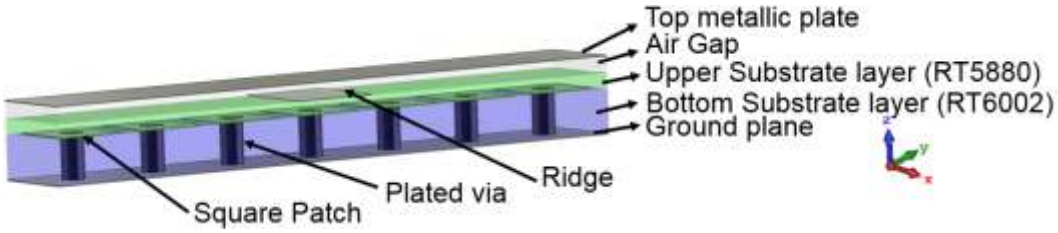

(a)

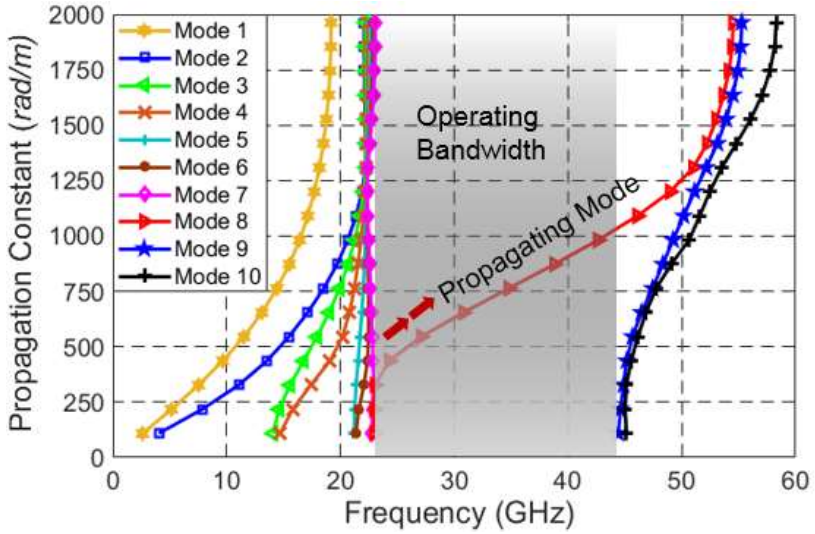

(b)

Figure1-20. (a). Configuration of a single row of modified SIGW consists of two layers of substrate and air gap. (b). Dispersion diagram of modified SIGW consists of semi-periodic plated vias and short-circuited ridge.

1.9. Objectives

The objective of this work is to introduce a novel design of the LWAs for the millimeter-wave frequency band applications. One of the common problem for the LWA is that usually, this kind of antenna does not have acceptable performance for the millimeter-wave frequency band. RGW technology as low-loss transition introduced for the millimeter-wave frequency band. The printed version of this technology which is called PRGW has promising performance and lower cost compared to the RGW, SIW and CRLH technologies for the millimeter-wave frequency band. This thesis work presents three designs of the LWAs based on the PRGW technology. The first objective is to design a periodic structure which has leaky modes that can be propagated in the desired operating frequency band. The second objective is to design a low-loss and wideband transition in order to use the whole bandwidth supported by the unit cell. The third goal of this thesis is to introduce a new design of the LWA based on the analysis of the periodic structure. In addition, two array designs based on the SIGW technology introduced. All these works which are presented in this thesis can be scaled to any frequency band. In addition, all the proposed LWAs designed for the WiGig applications, which are more preferred for the communication companies and their requirements.

1.10. Thesis Organization

The thesis is divided into five chapters. This chapter discusses the concept of the soft and hard surfaces and the advantages and disadvantages of the different EBG unit cells which can be used in the RGW, PRGW, and SIGW. The coming chapter presents the basic concepts of the leaky-wave antennas (LWA) and their field behavior. In addition, for a periodic structure, a Brillouin diagram have been discussed in order to find out which of the space harmonics can act like a leaky wave. Chapter three introduced the periodic structure that used in the design of the LWA. Furthermore, a quasi-TEM transition and a transition from microstrip to the SIGW are presented. The slots of the proposed LWA designed in order to have an almost constant leakage ratio (α/k_0) which results in an almost constant gain. The proposed antenna has a wide impedance bandwidth, high radiation efficiency, high gain with no sidelobe level. In chapter four a power divider and two linear array antennas presented. Both array designs can achieve 3 dBi

higher gain. In addition, a new termination has been considered which resulted in a shorter physical length of the anenna. Last chapter summarized the results obtained in this thesis and suggested furture developments.

Chapter 2

Leaky-Wave Antenna and Fields Behavior

2.1. Introduction

Leaky wave antenna (LWA) is a class of antennas that belongs to the family of traveling-wave antennas [36]. The first LWA was introduced by W.W. Hansen in 1940 [37]. The guiding structure of LWA is similar to the pipeline of water with some holes in the longitudinal axes. When water goes through the pipeline, we observe that the leakage from the holes occurs [38]. In the LWA instead of water the power leaks continuously. LWA is a waveguiding structure that radiates by progressively leaking its energy out to free space from a traveling wave with a phase velocity larger than the speed of light. Because of the leakage of power, the propagation wavenumber $(k_z = \beta - j\alpha)$ on the guiding structure has complex value, consisting of phase constant β and an attenuation constant α where the phase constant controls the beam angle and the attenuation constant controls the beamwidth and radiation efficiency [39]. The aperture distribution may be tapered to control the sidelobe level or the beam shape [40]. Most of the initial LWA is based on a closed waveguide where the leakage has been obtained by adding a long longitudinal slot in the narrow wall of the waveguide as shown in Figure. 2-1. LWA has the ability to produce a fan beam, pencil beam and conical beam which can be used in many applications such as radar system applications for detecting the objects [41] and it is very suitable for an image processing application [42]. The fan beam has also been used with a Luneberg lens as a feed of the high gain reflector antenna for millimeter-wave frequencies [43]. The LWA is widespread among antenna engineers because of its several advantages over slot array and phased array antennas. LWA can easily achieve a beam scanning without any need of phase shifters which is necessary for phased array antennas. Plus the radiating elements of LWA can be easily excited without any need for the complicated and bulky feeding network as used in regular array antennas, which have the ability of beam steering. Therefore, LWA can reach a lower fabrication cost. In addition, in the slot array antenna, the scan range is limited because of the use of resonant slots (frequency dependent slot). While with the metamaterial–

based LWA, a wide range scanning can be easily obtained [44], [45] and [46]. However, using metamaterial structure adds more complexity to the antenna for the millimeter-wave frequency band. In addition, SIW-based LWAs suffer from a large gain variation [47], [48], [49] and low radiation efficiency [50].

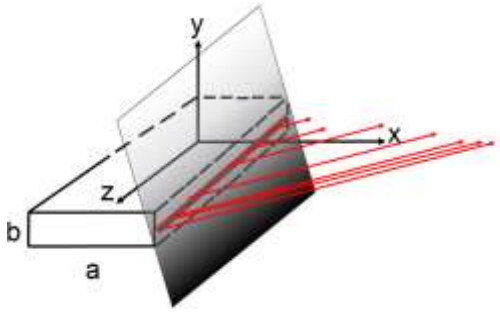

Figure. 2-1. Leaky-wave antenna consists of a rectangular waveguide with a long longitudinal slot (an infinite ground plane is shown surrounding the slot).

We can categorize the LWA according to their geometry and principle of operation and shape of the radiation pattern. We can divide LWA to the one-dimensional (1D) LWA and two dimensional (2D) LWA. Another classification is according to the structure of LWA, which can be uniform, quasi-uniform, or periodic. A brief discussion about the different type of LWA will be addressed in the following sections.

2.2. One-dimensional Uniform Leaky-Wave Antenna

The geometry of the one-dimensional uniform LWA has been shown in Figure. 2-2 (a). This structure consists a rectangular waveguide that has long slit to allow the power to leak. The width of the slit must be much narrower than the height of the waveguide [51]. Therefore, it causes only a small perturbation of the fast-wave TE_{10} dominant mode with propagation constant $\beta_{10}^{\mathrm{TE}} = \sqrt{k_0 - \pi/a}$. The structure in Figure. 2-2 supports a wave travelling along the longitudinal slot and, it can be assumed as a uniform structure because the geometry of it does not change in the longitudinal (z axis). However, the slot can be tapered to improve the side lobe level. If we feed the waveguide from one side, then, we have regular conical-shaped fan beam in the radiation hemisphere due to the baffle which is larger than the wavelength. The corresponding radiation pattern is in the forward quadrant $(z > 0)$ due to the phase constant which is always positive and nonzero $\beta > 0$ for all frequencies, since $\beta = k_0\sqrt{\varepsilon_{re}}$

with ε_{re} > 0, and therefore they are restricted to forward radiation excluding broadside. When the beam angle approach 90° or in other words, we have broadside beam, then the shape of the radiation pattern change to the narrow beam donut type of pattern. It is difficult to obtain a beam at broadside due to the cutoff of the waveguide. To obtain a broadside radiation pattern we can feed the waveguide from both sides or excite the waveguide in the middle. Then, we have two beams in both sides of broadside ($\beta \gg \alpha$) and if the structure is properly designed then these two beams near broadside can merge and form a single broadside beam ($\beta < \alpha$). However, [52] shows that a ferrite loaded waveguide can easily obtain a broadside radiation pattern. In addition, to obtain a pencil beam type of radiation, we can use 1D-LWA as a linear array [53].

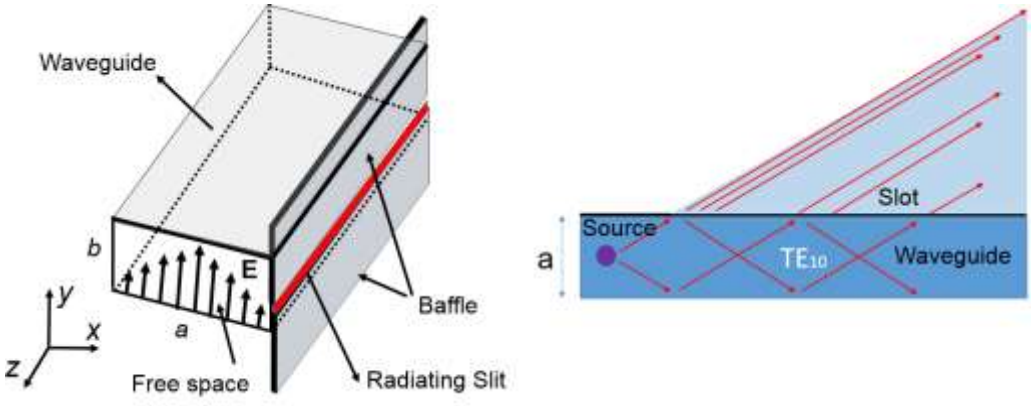

Figure. 2-2. One-dimensional uniform leaky-wave antenna.

2.3. One-dimensional Periodic Leaky-Wave Antenna

Periodic leaky-wave antenna (PLWA) is a structure consisting of periodic modulation (in the form of periodic discontinuity) for one of their features (slots, metallization, permittivity or permeability) along the axis of propagation. An example of PLWA is shown in Figure. 2-3. The structure consists a rectangular waveguide filled with dielectric material and has a periodic array of radiating holes in the narrow wall of the waveguide [54]. Due to the presence of the dielectric, the fundamental space harmonic associated with the dominant TE_{10} mode $\beta_{10}^{\mathrm{TE}} = \sqrt{\varepsilon_r k_0^2 - (\pi/a)^2}$ is generally a slow wave. This mode does not radiate, but it needs the periodic modulation to produce the radiation. According to Bloch-Floquet theory, PLWA supports an infinite number of space harmonics (Floquet waves) due to their periodicity [55] where the relation between the space harmonics represented as $\beta_n(\omega) = \beta_0(\omega) + 2\pi n/p$ (p is the period and n is an integer). The n^{th} Floquet wave has a wavenumber given by $k_{zn} = k_{z0} + 2\pi n/p$ and the wavenumber of the fundamental Floquet ($n = 0$) wave given by $k_{z0} = \beta - j\alpha$.

The main ($n = 0$) space harmonic is generally a slow wave. Therefore, it does not radiate significantly in most PLWAs. Instead, one of the higher space harmonics (usually $n = -1$) is designed to be a fast wave. So that, $-k_0 < \beta_{-1} < k_0$ and hence, this space harmonic is a radiating wave. Compared to the uniform LWA, PLWA can scan from the backward to forward quadrants due to $-k_0 < \beta_{-1} < 0$ or $0 < \beta_{-1} < k_0$, respectively (or more precisely the angle of radiation pattern is related to the imaginary part of wave number). In PLWA the beam will scan with frequency. In both backward and forward quadrants, the beam has a conical shape. However, at broadside, the shape of the beam changes to donut-shape and the beamwidth of the antenna dramatically changes. In the most PLWA usually at broadside, the input match degrades as the main beam reaches broadside. In addition, at this point usually all the slots (periodic discontinuity) of PLWA are in phase and we have standing waves instead of travelling waves and the attenuation constant drops to zero due to the open stopband (matching is pure and $\beta_0 p = 2\pi$) which is discussed in the following sections.

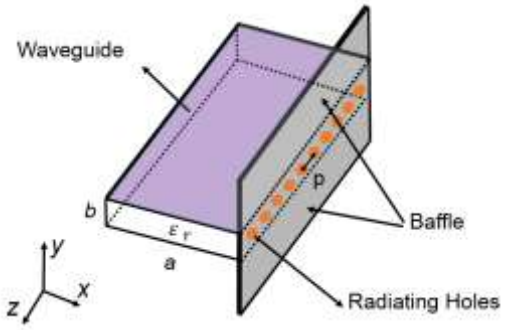

Figure. 2-3. Dielectric-filled rectangular waveguide with a periodic array of holes in the narrow wall of the waveguide and ground plane baffle.

Another type of PLWA is shown in Figure. 2-4.This structure is a microstrip array, which consists of transverse strips radiate in the perturbed TM_0 surface-wave mode of the grounded slab [56]. Leakage into the surface wave will occur when the wave is fast with respect to the surface wave ($|\beta| < k_{\mathrm{TM}_0}$), where $k_{\mathrm{TM}_0}$is the wavenumber of the surface wave. The proposed structure can scan from the backward to forward quadrants due to the periodicity of the strips (p). This structure has the ability to produce a fan beam or a pencil beam. The pencil beam is achieved when the 1D-PLWA is used as an element in an array, or in other words, when we have an electrically large transverse aperture, this kind of beam can be easily achieved. The pencil beams may be scanned over all quadrants of the hemispherical space, except near broadside due to the open-stop band.

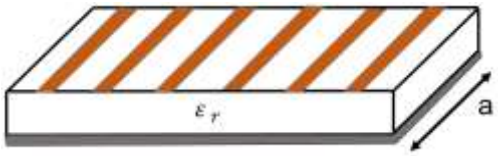

Figure. 2-4. Microstrip array of transverse strips acting as a periodic leaky-wave antenna that radiates from the perturbed surface-wave mode.

2.4. One-dimensional Quasi-Uniform Leaky-Wave Antenna

Another type of LWA is quasi-uniform LWA. This kind of antenna is electromagnetically similar to the uniform LWA. However, their topology is similar to the PLWA. Their structure is similar to the structure in Figure. 2-3 and Figure. 2-4 within the difference that the periodicity is much smaller than the guided wavelength of traveling wave ($p \ll \lambda_g$) [57]. Compared with uniform and PLWA in quasi-uniform LWA, the fundamental space harmonic ($n = 0$) is responsible for the radiation which can be a fast wave in specific frequencies. The holey waveguide antenna shown in Figure. 2-3 with subwavelength spacing between the holes becomes a quasi-uniform antenna radiating from the fundamental space harmonic of the perturbed TE_{10} waveguide mode, provided the permittivity is low enough so that the TE_{10} waveguide mode is a fast wave [58]. The radiation pattern of quasi-uniform LWA is limited to the forward quadrant and, it is similar to the uniform LWA. However, by using metamaterial-based LWA, a wide range scanning can be easily obtained [44], [45] even through the broadside due to the elimination of stopband (when we have balanced mode).

2.5. Field Behavior of Leaky Waves

The radiation for the LWA is usually due to a mode referred to as a leaky mode, which is a guided mode that leaks and radiates the power along the structure. [59]. For a uniform LWA, the guiding mode is a single fast wave ($0 < \beta < k_0$) and having a complex number $k_z = \beta - j\alpha$. In PLWA the guided mode consists of an infinite number of space harmonics with the wave number $k_{zn} = \beta_n - j\alpha$ where $\beta_n = \beta_0 + 2\pi n/p$. The $n = 0$ is the fundamental space harmonics, which carries most of the power while the $n = -1$ space harmonics is usually the one that causes radiation ($-k_0 < \beta_{-1} < k_0$) through specific frequencies. In the PLWA, if the attenuation constant α assumes to have a positive value, then according to the periodicity between the elements or the value for the β_{-1}, the radiation pattern could be in the forward or backward quadrant. We have a forward wave ($\beta_{-1} > 0$) when the phase and the group velocity

of radiating space harmonic (for example $n = -1$) are in the same direction and we have a backward wave ($\beta_{-1} < 0$) when the phase and group velocity of radiating space harmonic are in the opposite direction of each other. If we model the LWA of Figure. 2-2 as a magnetic line source, then the radial wave number (vertical wavenumber) given by $k_p = (k_0^2 - k_z^2)^{1/2}$. Therefore, due to the complex value of k_z there are two possible solutions for the value of k_p:

$$k_p^2 = k_0^2 - k_z^2$$
$$(\beta_p - j\alpha_p)^2 = k_0^2 - (\beta_z - j\alpha_z)^2$$

$$\beta_p^2 - \alpha_p^2 - j2\beta_p\alpha_p = k_0^2 - \beta_z^2 + \alpha_z^2 + j2\alpha_z\beta_z$$

If we take the imaginary part, then we have $\beta_p\alpha_p = -\beta_z\alpha_z$. If $\beta_{-1} > 0$ (radiated space harmonic) and $\alpha > 0$ then the field will exponentially increase in the radial direction and the power radially outward so we have an improper field as shown in Figure. 2-5. For the proper field the $\beta_{-1} < 0$ and the field will be exponentially decaying in the radial direction and the power is radially inward as shown in Figure. 2-6. For the slow waves $|\beta| > k_0$ for both forward and backward and we have a proper field. However, for the fast waves $|\beta| < k_0$ and we have a proper field for the backward wave and an improper field for the forward wave.

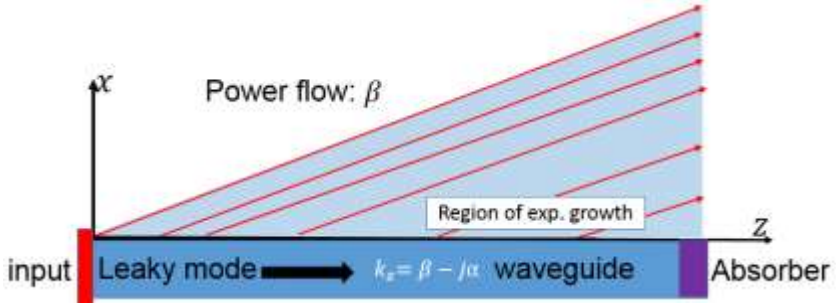

Figure. 2-5. Ray picture of the forward leaky wave for a dielectric holly waveguide of the structure in Figure. 2-3 [59].

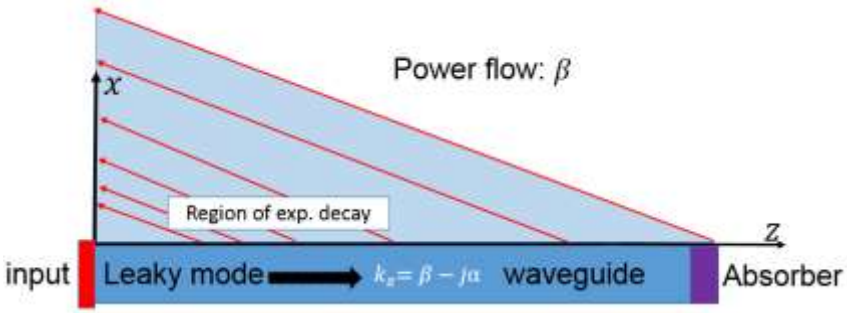

Figure. 2-6. Ray picture of the backward leaky wave for a dielectric holly waveguide of the structure in Figure. 2-3 [59].

2.6. Physics of Leaky Waves

For a strong leaky mode, the wavenumber must be in the physical region where the wave is a fast wave. In LWA in order to radiate the power, we must have a leaky mode that has complex wavenumber, and it must be in a physical region and be fast wave ($\beta < k_0$). A leaky-mode is considered to be physical if we can measure a significant contribution from it. In contrast, leaky waves are not physically important if they are slow waves (waves radiate only at discontinuities). For a grounded dielectric slab the leaky modes usually can be obtained from a surface-wave modes. If we assume that we have a surface - wave mode with a nonzero cutoff frequency, then a nonphysical complex leaky mode is achieved at sufficient low frequency [60]. Any mode other than TE_1 surface-wave mode (which remains real improper surface wave mode at all frequencies below cutoff frequency) and TM_0 surface-wave mode (which has zero cutoff frequency and it can propagate at any frequency) can transform to a complex leaky mode. The cutoff frequency is the transition between a proper and improper mode (cutoff for TM_1: $v = 0$, $u = \pi$) which is shown in Figure. 2-7(below the cut off frequency the mode has nonphysical behavior up to f_p).

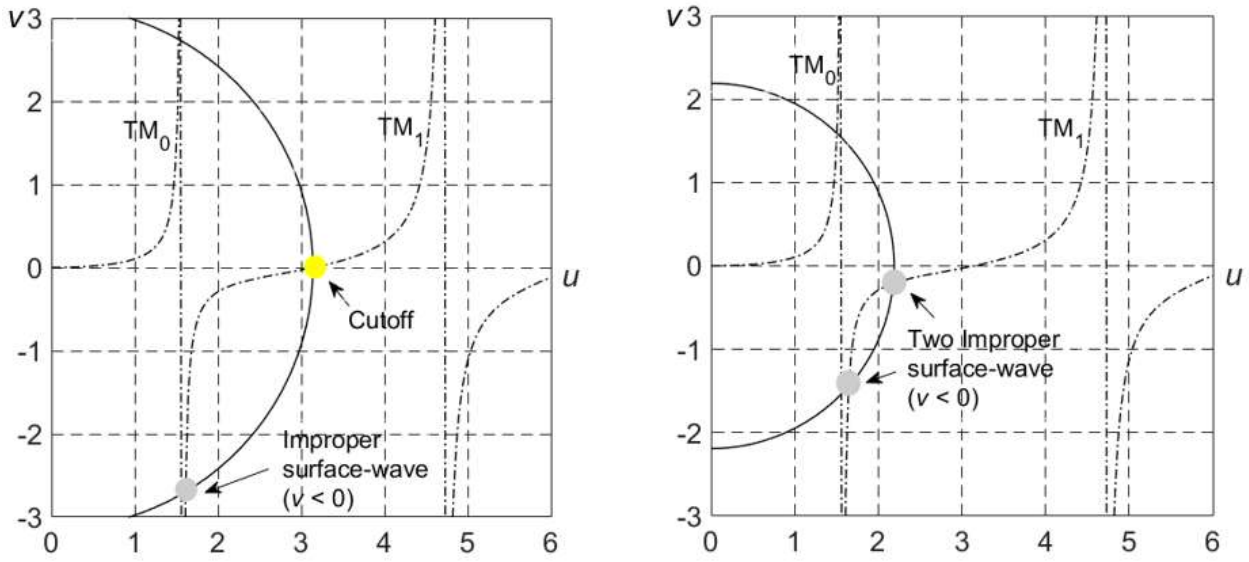

(a) (b)

Figure. 2-7. (a). Cutoff frequency ($v = 0, u = \pi$) of TM_1 ($f = f_c$), there is also an improper surface-wave mode ($\varepsilon_r = 15$, h = 0.254 mm, $f = 157.6$ GHz). (b). Two improper surface-wave modes ($\varepsilon_r = 15$, h = 0.254 mm, $f = 110$ GHz).

Above the cutoff frequency, we have a slow wave ($\beta > k_0$) and the wave decay exponentially (proper wave). As the frequency gets lower the normalized phase constant (β/k_0) decreases and reaches the value 1 at the cutoff frequency. At the frequency range below the cutoff the phase constant start to increase and in a lower frequency (splitting point ($f_s < f_c$) Figure. 2-8) the two nonphysical improper real surface-wave modes merge together. As a result, below the splitting point, the real wavenumbers change to complex wavenumbers and we have a complex improper leaky mode. Below the splitting point, one of the wavenumber has the form $k_z = \beta - j\alpha$ and another one has complex conjugate of the other. The attenuation constant is zero for the frequency above f_s and it starts to increase for the frequency below f_s [61]. If we track the wavenumber with the form $k_z = \beta - j\alpha$, we will see that as the frequency gets lower, the phase constant usually decreases until it reaches f_p where $\beta = k_0$. The frequency range between f_c and f_p refers to the spectral-gap region where the mode is nonphysical. Above the spectral-gap region, we have physical surface waves, which carry power but it does not radiate. Below the spectral-gap region, we have a complex physical leaky mode, which can radiate the power and it is a fast mode ($\beta < k_0$). At a frequency lower than f_p, which refers to f_l the physical

complex, improper fast mode change to nonphysical complex slow mode as shown in Figure. 2-9. The attenuation constant increases dramatically below the quasi-cutoff frequency where we have the maximum power density ($\beta = \alpha$) [61].

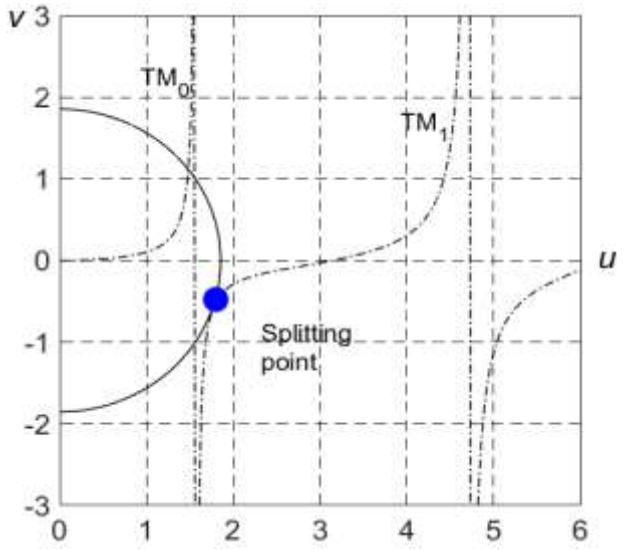

Figure. 2.8. Splitting point ($f = f_s$ = 93.2 GHz, ε_r = 15, *h* = 0.254 mm), two improper surface-waves merge.

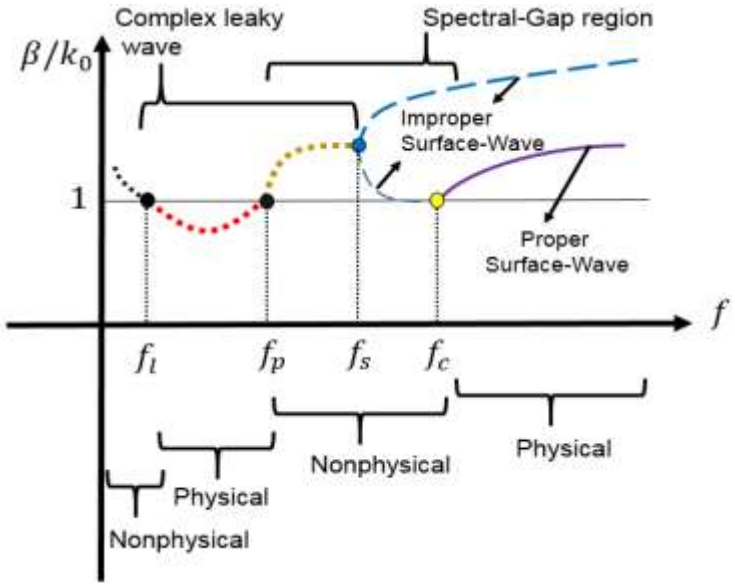

Figure. 2-9. Behavior of normalized phase constant for leaky mode for a grounded dielectric slab [59].

2.7. Bidirectional Leaky-Wave Antenna

A bidirectional LWA has the ability to produce two equal beams in both forward quadrant and backward quadrant region [59]. The feeding part of bidirectional LWA is usually in the center of the structure, and typically they use two match loads or absorbers at the end of the antenna. If the beam angle for one beam is at $\theta°$, another beam usually appears at $\pi - \theta°$. Thus, when θ approaches 90°, then the two beams can merge with each other and make a single beam. The angle of the beam can be obtained from $sin\theta = \beta/k_0$ when the phase constant is much bigger than the attenuation constant ($\beta \gg \alpha$). However, this formula is not very accurate for the frequency near splitting point $\beta = \alpha$ and the angle, of the beams, can be obtained from $\theta_{1,2} = \pm\sqrt{\beta^2 - \alpha^2}$ [62]. At the splitting point the beam has two close peaks with a dip in the middle (not null), but off a broadside, as shown as in Figure. 2-10. In addition, at this point usually, we have a maximum power density (for lossless structure). This condition is set for slotted parallel-plated waveguide. However, in [63] shows that for a lossy structure of a periodically loaded transmission line, the absolute value of the phase constant is smaller than the attenuation constant when we have a maximum power density. The single broadside beam can be achieved when the phase constant is smaller than the attenuation constant ($\beta < \alpha$) and the narrowest broadside beam can be obtained when $\beta/\alpha = 0.518$ and the beam made narrower by a factor 0.841 compared to the case where the power density is maximum at broadside [62].

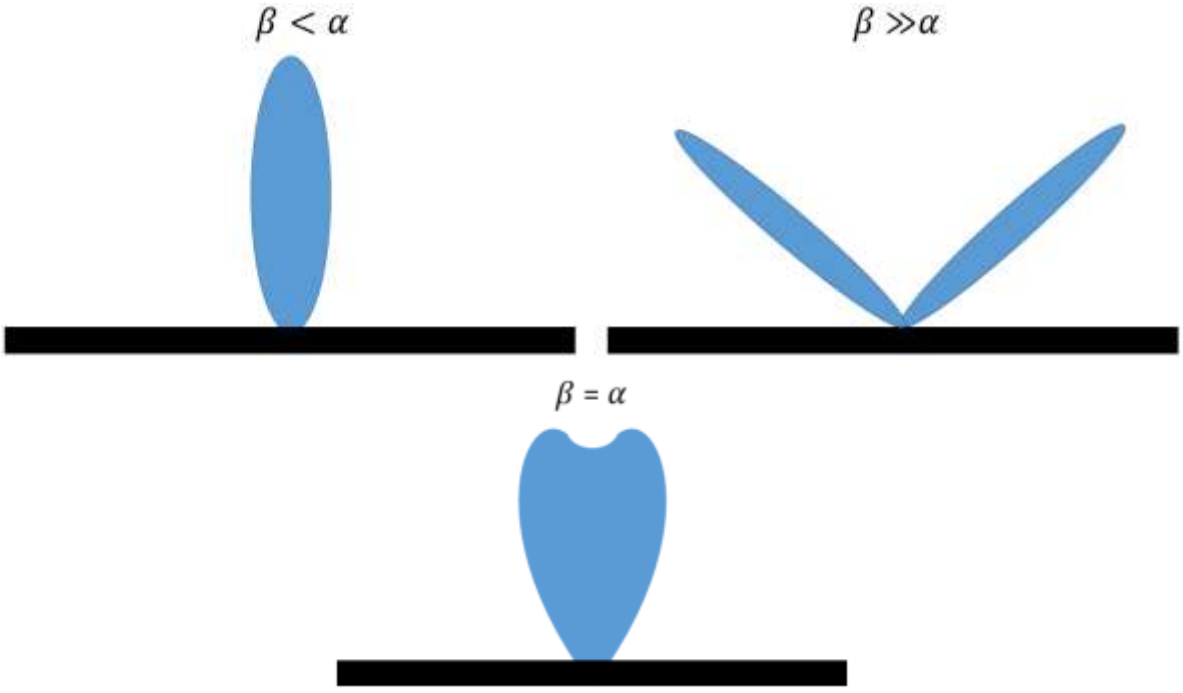

Figure. 2-10. The relation between phase and attenuation constant and radiation pattern when we fed the LWA from the center.

2.7. Brillouin Diagram Analysis

Another tool that usually used to analyze the wave of the PLWA is Brillouin diagram, which is a graphical representation of the dispersion relation of the space harmonic axial phase constants. The Brillouin diagram of a periodic structure (metal strip grating on a grounded dielectric slab) is shown in Figure. 2-11. For a reciprocal periodic structure ($\beta_0 \leftrightarrow -\beta_0$), the Brillouin diagram is symmetric with respect to the ordinate axis ($\beta_n p \,/\, \pi = \; n, n = 0, \pm 1, \pm 2$). The blue part in Figure.2-11 refers to the bounded-wave region. In this region, all the spatial harmonics are simultaneously slow ($k_0 p < \pi$). As mentioned before a LWA usually suffers from no broadside radiation. When we have near broadside radiation in PLWA, usually all the slots are in phase with $\beta_{-1} = 0$ (or $\beta_0 p = 2\pi$) and instead of having a travelling wave we have a standing wave. The attenuation constant usually drops to zero near this point which is referred to as open stopband and it is exactly zero at $\beta_0 p = 2\pi$ which is referred to as stopband null point. Another stopband occurs at $\beta_0 p = \pm\pi$ which referred to as closed stopband is. At closed stopband, the attenuation constant does not drop to zero. However, at the edge of the close stopband, the attenuation constant is exactly zero [62]. At close stopband, the overall mode is not leaky mode and the mode does not carry the power due to the bounded region. For metal-strip grating on a grounded dielectric slab the nth spatial harmonic is axially fast only if the corresponding point ($\beta_n p \,/\pi, k_0 p \,/\pi$) of the dispersion curve is located inside the fast wave region (FWR) and the nth spatial harmonic is axially slow only if the corresponding point ($\beta_n p \,/\pi, k_0 p \,/\pi$) of the dispersion curve is located outside of the FWR as shown in Figure. 2-11.

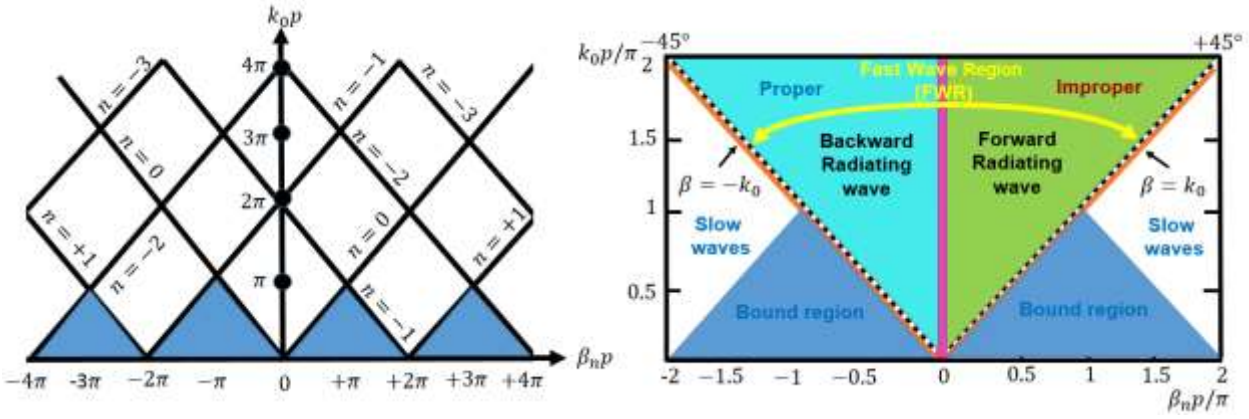

(a) (b)

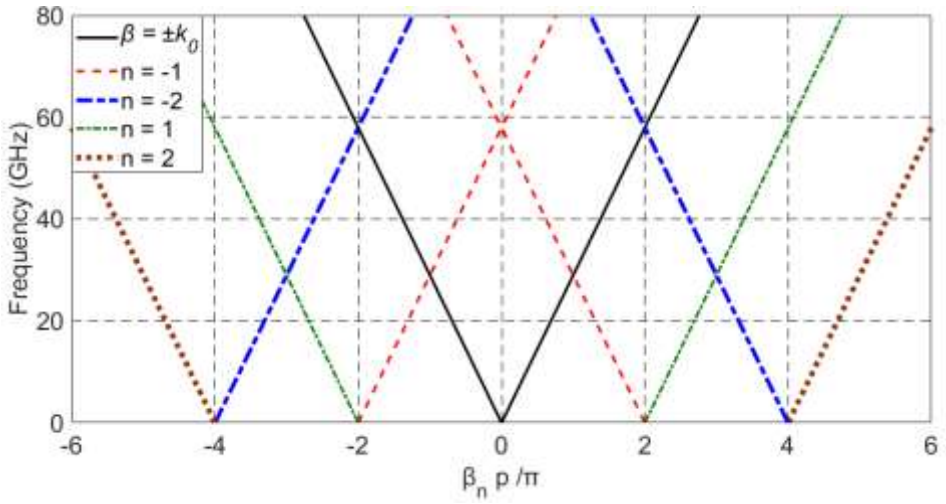

(c)

Figure. 2-11. (a). Brillouin diagram for a periodic structure (the region with blue color shows the bounded region), and (b) Forward and backward wave in the Brillouin diagram, and (c) An example of the Brillouin diagram for periodic structure (metal strip grating on a grounded dielectric slab) with the periodicity equal to p = 0.425 mm with $\varepsilon_r = 2.2$.

Chapter 3

Substrate Integrated Printed Ridge Gap Waveguide Leaky-Wave Antenna for WiGig Application

3.1. Introduction

In this chapter, we introduce a novel design of an LWA based on ridge gap waveguide (RGW) technology. The printed version of the gap waveguide technology known as printed ridge gap waveguide (PRGW) has been developed in [32] in which the PMC surfaces has been realized by printed mushroom surfaces. As ensuring the thin air gap height for PRGW structures at the millimeter waves is becoming a problem for large structures. Therefore, the gap is filled with a thin low loss substrate layer in order to have a fixed gap height between the PEC and

AMC layers all over the structure. This modified version of PRGW called substrate integrated gap waveguide (SIGW) introduced in [34], in which a thin substrate is filling the gap to fix the gap height all over the circuit. As mentioned in the previous chapter, the LWA usually suffer from large gain variation and low radiation efficiency especially in the millimeter-wave frequencies due to the dissipation factor, radiation leakage, and high insertion losses, which results in deteriorating the performance of the antenna. In this chapter, a new design of LWA based on SIGW technology is introduced. The objective is to design an LWA which has a high radiation efficiency and almost a stable gain for the whole operating frequency of the antenna. The proposed SIGW-LWA is a kind of 1D-periodic LWA which has no side lobes, high radiation efficiency, and almost a stable gain all the scanning frequency range of the antenna. The proposed antenna is designed for the WiGig application and fabricated on a two-layer substrate which is fed by a transition from microstrip to SIGW. In this chapter, we explain the steps of a prototype of SIGW-LWA and simulations and measurement results of proposed antenna are illustrated.

3.2. Substrate Integrated Gap Waveguide Configuration

For the desired IMS band, a printed periodic EBG must be designed. The first step is to design the unit cell that will provide the EBG within the IMS band. The unit cell structure and its dispersion diagram utilized in SIGW-LWA are shown in Figure. 3-1 and Figure. 3-2, respectively. The mushroom unit cell has a rectangular patch grounded by a plated via and covered by a dielectric substrate, which is topped by a conductor. Rogers RT5880 substrate with the dielectric constant of 2.2 is used for the upper layer, and Rogers RT6002 with the dielectric constant of 2.94 is used for the lower layer. The factors that affect the band gap provided by the periodic structure of this unit cell are the layer thicknesses, periodicity, and mushroom dimensions. A detailed study to investigate these factors can be found in [31]. The band gap of the designed cell is from 31.4 to 70.8 GHz.

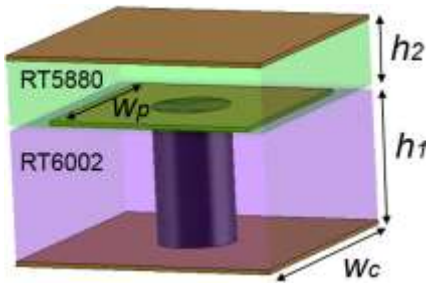

Figure 3-1. Unit cell dimensions h_1 = 0.508, h_2 = 0.254, Wp = 0.819, Wc = 1.05 (dimensions are in mm).

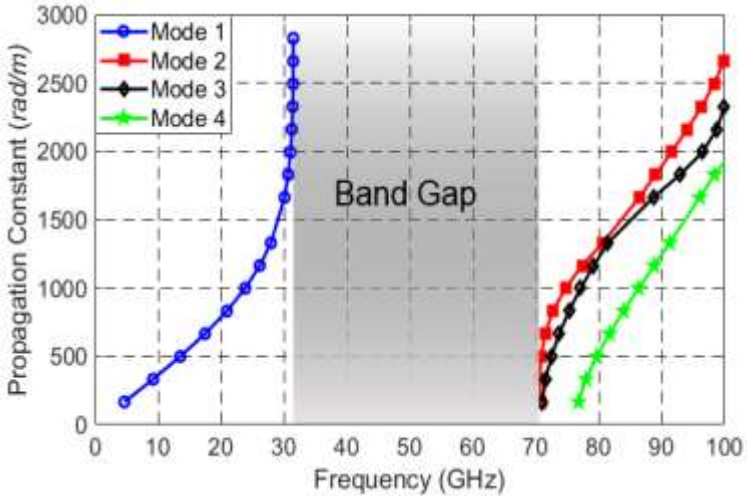

Figure 3-2. Dispersion diagram of the unit cell.

In order to show the guiding characteristics of the SIGW, a single line of SIGW surrounded from both sides by three rows of cells is considered. However, for this study, it is sufficient to study the dispersion diagram of one cell transverse to the line as shown in Figure. 3-3. To suppress any possible leakage of the signal under the ridge, a single row of metallic vias is included under the ridge to ground the ridgeline. The thin substrate filling the gap height is holding the upper conducting plate over the structure. The dispersion analysis of the SIGW line is shown in Figure. 3-4 showing the single quasi-TEM propagating mode along the ridge in the stopband of the periodic structure. The cutoff region provided by the AMC-PEC parallel plate decays the fields outside of the guiding region. The width of the ridge is tuned for a 50 Ω characteristic impedance of the line. The band gap, in this case, is smaller than the unit cell to be 32.3-67.8 GHz.

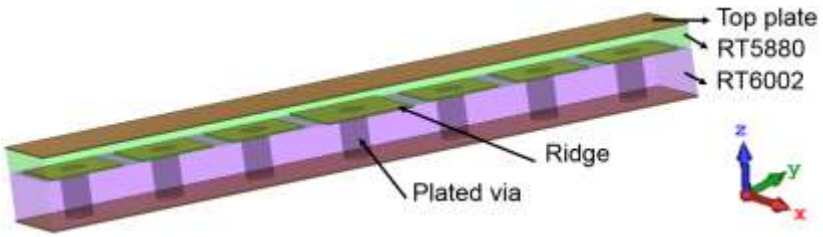

Figure 3-3. Configuration of layers for SIGW.

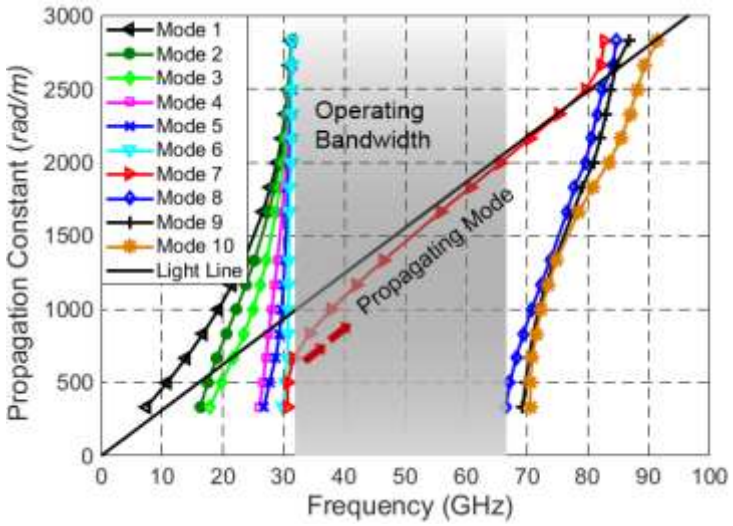

Figure 3-4. Dispersion diagram of SIGW line.

3.3. Slot Design of Substrate Integrated Gap Waveguide Leaky-Wave Antenna

The geometry of the SIGW-LWA is shown in Figure. 3-5, which consists of two layers of substrates. A periodic set of series centered transverse slots is applied on the top of the ground plane of the SIGW parallel to the guiding ridge. According to [47], to control and minimize the unwanted end reflections, tapered slots are added to both ends that also provide an ideal field in the uniform slots region. For tapering the slot, we used Chebyshev method, and in here we used 34 uniform slot and 8 tapered slots. The initial SIGW-LWA structure is excited by wave ports provided by the simulator. The wave ports are extended for almost one cell size around the guiding ridge to capture all fringing fields on both sides of the ridge. By varying the frequency, the phase constant and the electrical length between the slots also vary, which causes a change in the progressive phase between the slots. Therefore, the angle of the main beam is scanned by varying the frequency.

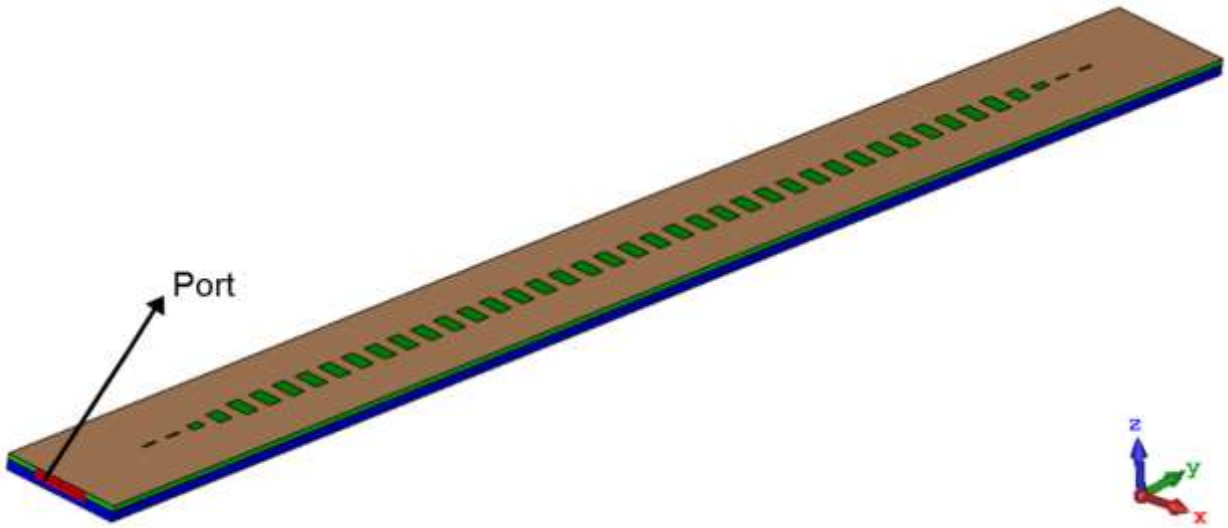

Figure 3-5. Configuration of SIGW-LWA.

The appearance of any grating lobes is avoided because the periodicity of the slots is considered to be less than a wavelength, which is 2.57 mm due to the dielectric filling. The length of the periodic slots is also set to be 1.67 mm, which is almost equal to half of the guided wavelength of the SIGW line. To uniformly excite these periodic slots through the SIGW line, the width of the ridgeline should be slightly wider than the slot length. For this design, the width of the propagating ridge under periodic slots is fixed to be 1.9 mm.On the other hand, the width of the periodic slots is designed to reach a low and almost constant value for the attenuation constant for all operating frequencies. Accordingly, we could obtain an approximately constant gain over the bandwidth due to the fixed amount of leakage per unit length. It should be mentioned that to decrease the effect of the fringing fields and to suppress any possible propagation under the guiding ridge, two rows of metallic vias are placed under the edge of the guiding ridgeline as shown in Figure. 3-6. The vias spacing and diameter are designed according to the conditions given in [48], which is $d / p > 0.5$, to have a minimum leakage of the waves under the ridgeline.

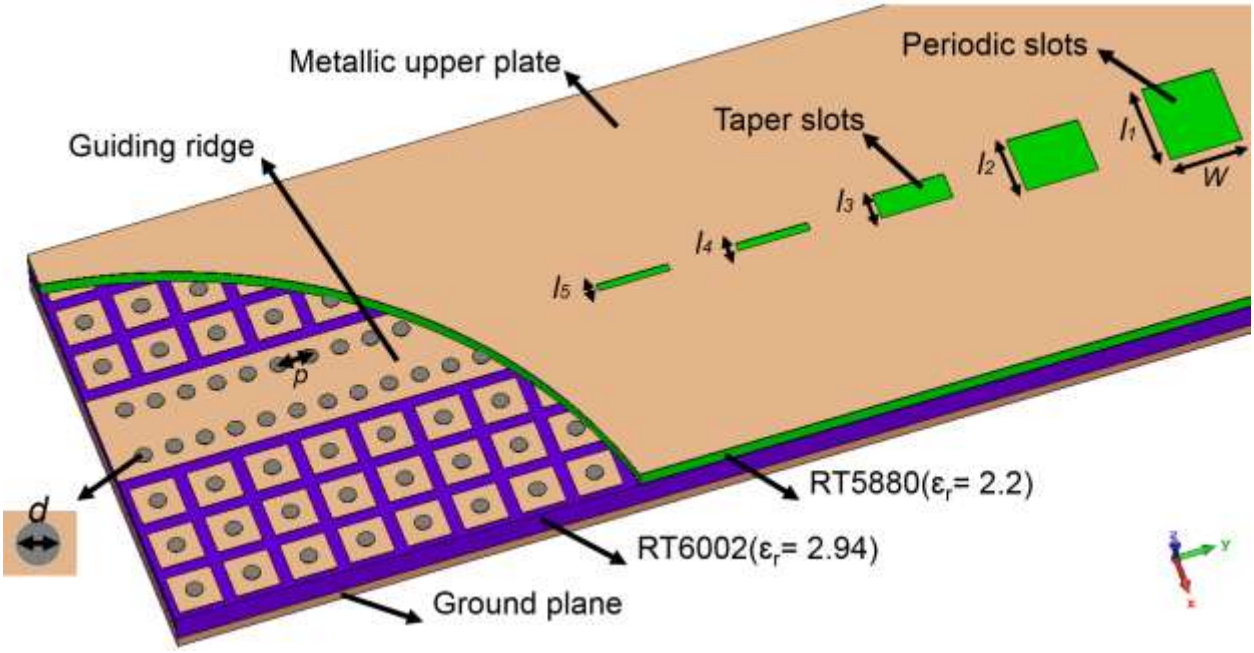

Figure 3-6. Configuration of SIGW-LWA (d = 0.3 mm, p = 0.56 mm, w =1.32 mm l_1 = 1.67 mm, l_2 = 1.85 mm, l_3 = 0.52 mm, l_4 = 0.18 mm, l_5 = 0.15 mm).

According to [64] and [65] for LWA with the normalized leakage constant $\alpha/k_0 < 0.02$ a length of 20 λ_0 is required to radiate more than 90% of power. Therefore, the length of the whole LWA including periodic section and tapered ends is fixed for this length. A parametric study is accomplished for different widths of the periodic slots to evaluate the performance of the LWA in terms of the reflection coefficient, normalized leakage constant, and gain as illustrated in Figure 3-7, Figure 3-8 and Figure 3-9, respectively. Based on these analyses, it has been seen that the slot width of 1.32 mm results in the most suitable design providing a relatively stable gain, constant leakage ratios less than 0.02, and wider impedance bandwidth with a reflection coefficient less than -20 dB for all over the frequency band. Therefore, based on this analysis, we expect to have a narrow beam for the antenna radiation pattern. The upper layer of the structure in Figure 3-6 is similar to the structure of a metal strip grating on a grounded dielectric slab. Thus, the angle and the type of wave can be predictable by using the Brillouin diagram of the structure of Figure 2-4. Figure 3-10 shows the Brillouin diagram for the periodic structure (p = 2.57 mm) of Figure. 2-4 which indicate that the n = -1 space harmonic can be act as a leaky wave for the range of the frequency of antenna operation (57-64 GHz). According to the analysis of Figure 3-10, we expected to have only one beam for our structure and the wave

expected to be a physical backward proper fast wave due to the negative value of the first space harmonic ($k_0 < \beta_{-1} < 0$) in the range of the operation frequency of the antenna and the power expected to flow inward radially.

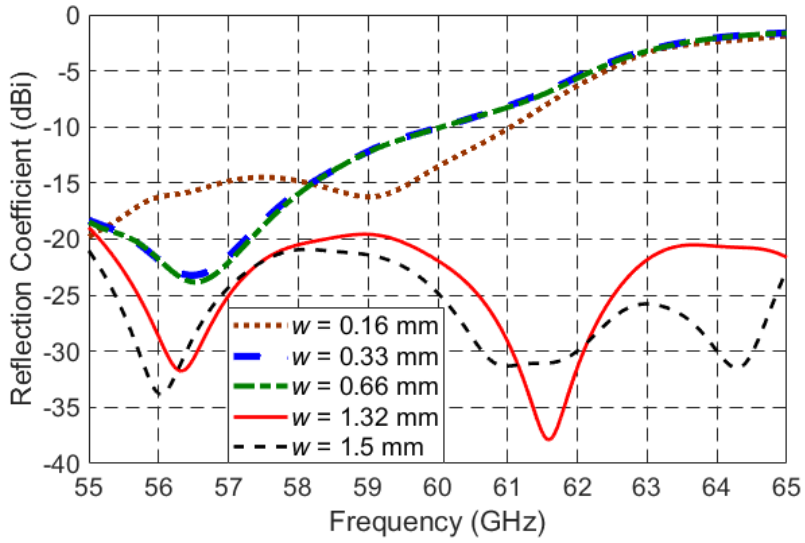

Figure 3-7. Reflection coefficient for different width of slots.

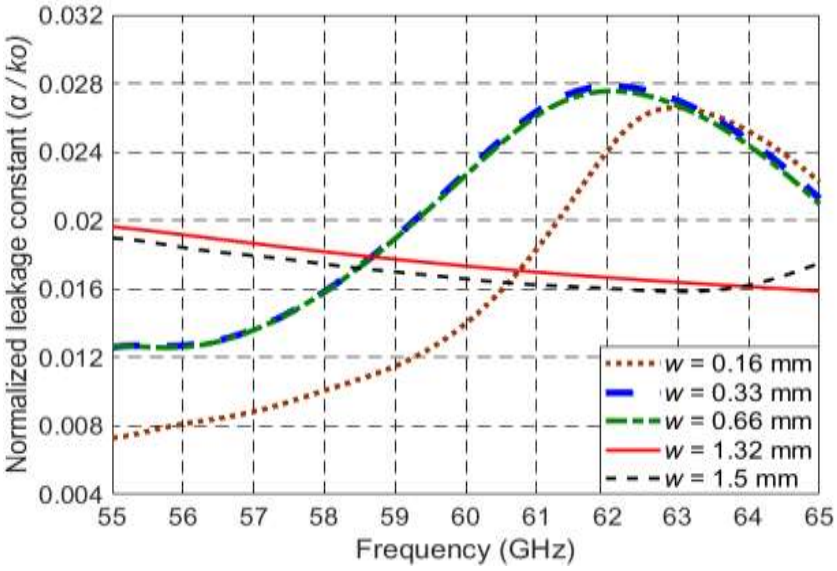

Figure 3-8. Normalized leakage constant for different width of slots.

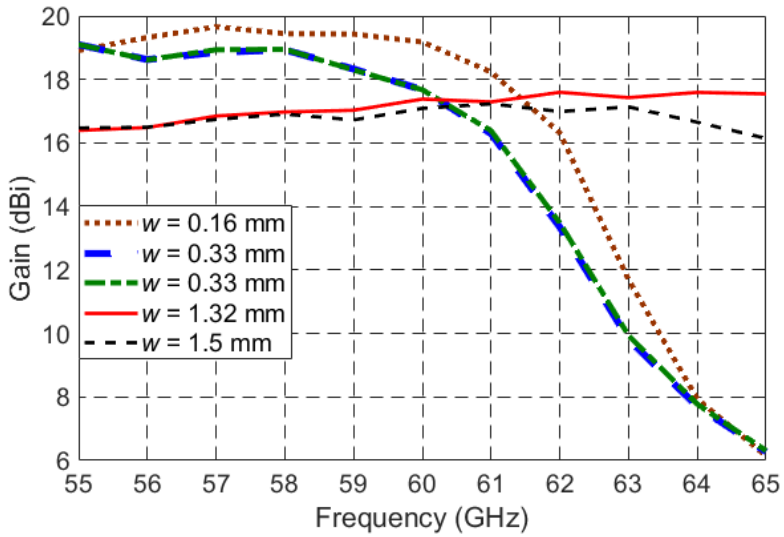

Figure 3-9. Realized gain for different width of slots.

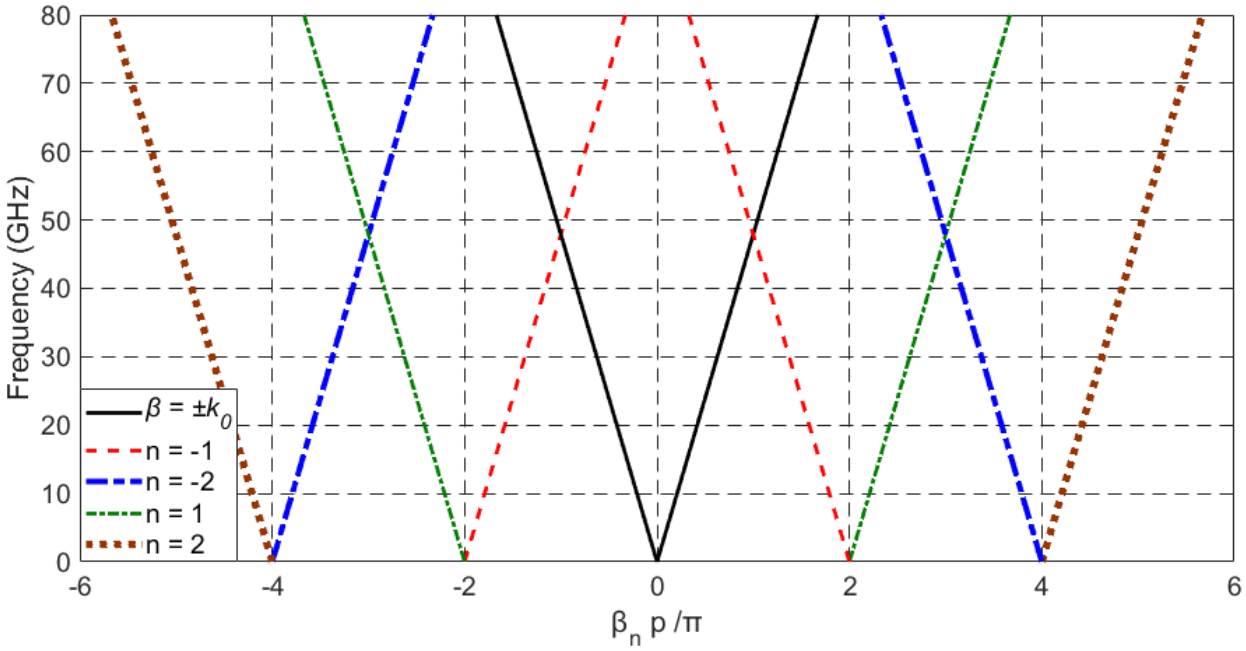

Figure 3-10. Brillouin diagram for the periodic structure (p = 2.57 mm) of Figure. 2-4.

3.4. Antenna Configuration with Transitions

As mentioned, the width of the ridgeline exciting the periodic slots is set to be 1.9 mm. This width of the ridge is corresponding to a characteristic impedance of 29 Ω. However, to excite the antenna through a standard connector for measurement purposes, it should be connected to a 50 Ω transmission line. Therefore, the designed LWA structure has to be matched to the 50 Ω

line. The PRGW structures can be easily excited by a microstrip line with the substrate thickness equal to the gap height of the PRGW [66]. To excite this LWA, first, a tapered transition is applied to match the wide ridgeline of LWA to the 50 Ω SIGW line, as shown in Figure. 3-11. This tapered SIGW transition is tuned to be long enough to cover a wide frequency band. As seen in the transition geometry, two sets of parallel vias are used close to the ridge edge to suppress the possible leakage under wide printed ridge. Along the tapered transition, the parallel vias are narrowed down to the single row under the 50 Ω SIGW line. Then, another transition is used to connect the 50 Ω SIGW to the 50 Ω microstrip line. The width of MS line is smaller than the width of the guiding ridgeline of SIGW-LWA in which the propagation is in the air (width of MS is 0.74 mm and width of the guiding ridgeline is 1 mm). A detailed study of this transition is given in [67]. The simulated *S*-parameter of the back-to-back connection with the whole transition is plotted in Figure. 3-12 which shows a good insertion loss response. Figure. 3-13 shows the total configuration and separated layers of SIGW-LWA with the tapered transition and the MS line. The electric field distribution inside the antenna starting from the feeding MS line is shown in Figure. 3-14. The tapered transition provides a relatively uniform field of quasi-TEM propagation of the ridgeline exciting the periodic slots. The fabricated prototype of the designed LWA antenna excited by end launch connectors is shown in Figure. 3-15. A 3D printed holder is prepared to support the antenna safely during the measurement.

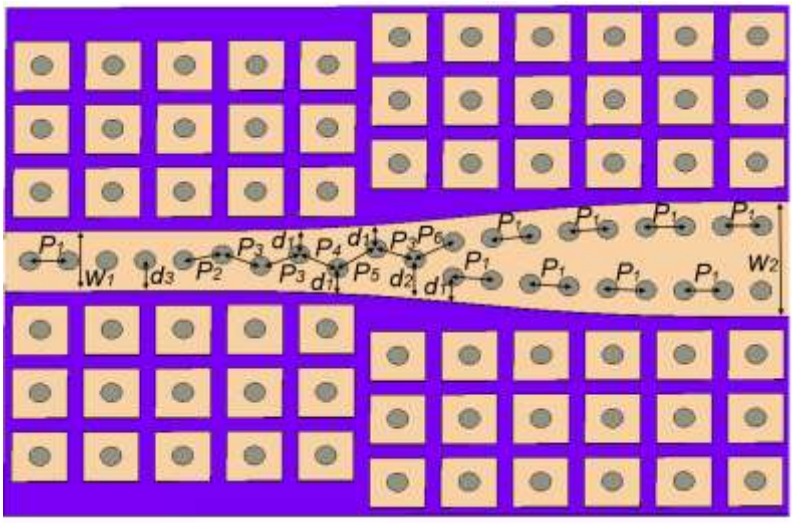

Figure. 3-11. Taper ridge transition of SIGW-LWA (d_1 = 0.26 mm, d_2 = 1.9 mm, d_3 = 0.37 mm, p_1 = 0.56 mm, p_2 = 0.57 mm, p_3 = 0.59 mm, p_4 = 0.62 mm, p_5 = 0.65 mm, p_6=0.63 mm, w_1 = 1mm, w_2 = 1.9mm).

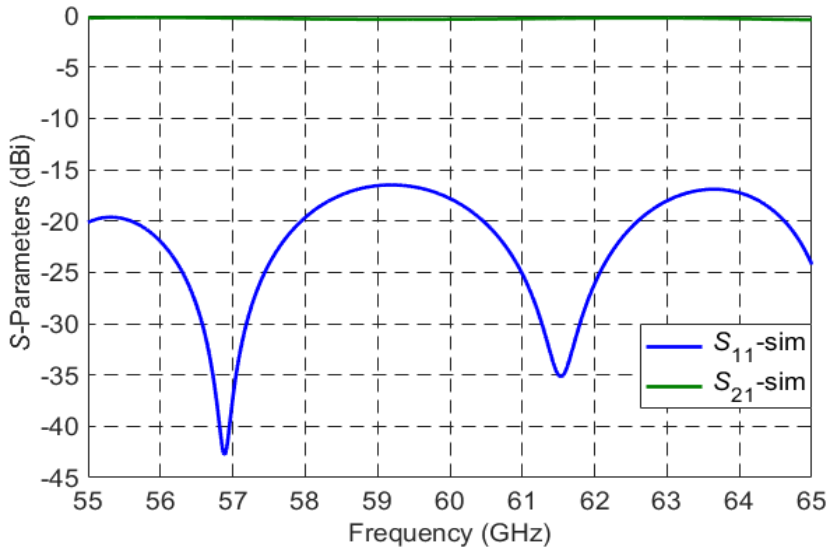

(b)

Figure. 3-12. Simulated *S*-parameter of the back-to-back 29 Ω SIGW to 50 Ω microstrip transition.

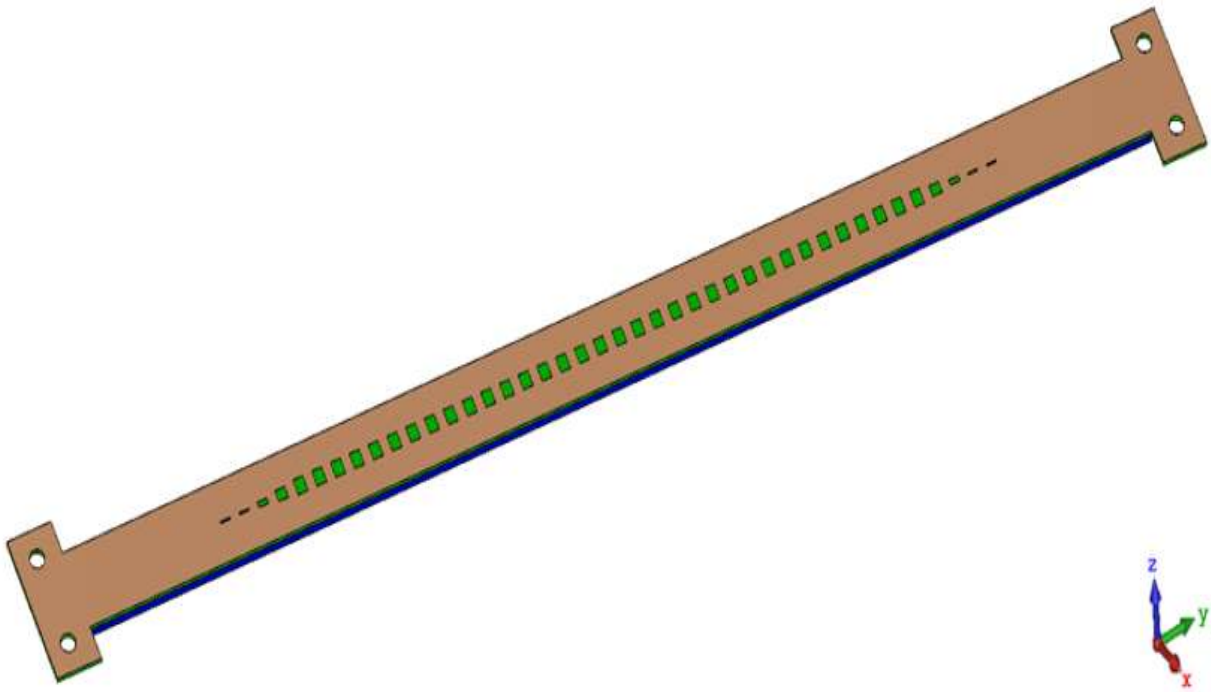

Figure. 3-13 (a).Total structure for SIGW-LWA with MS line.

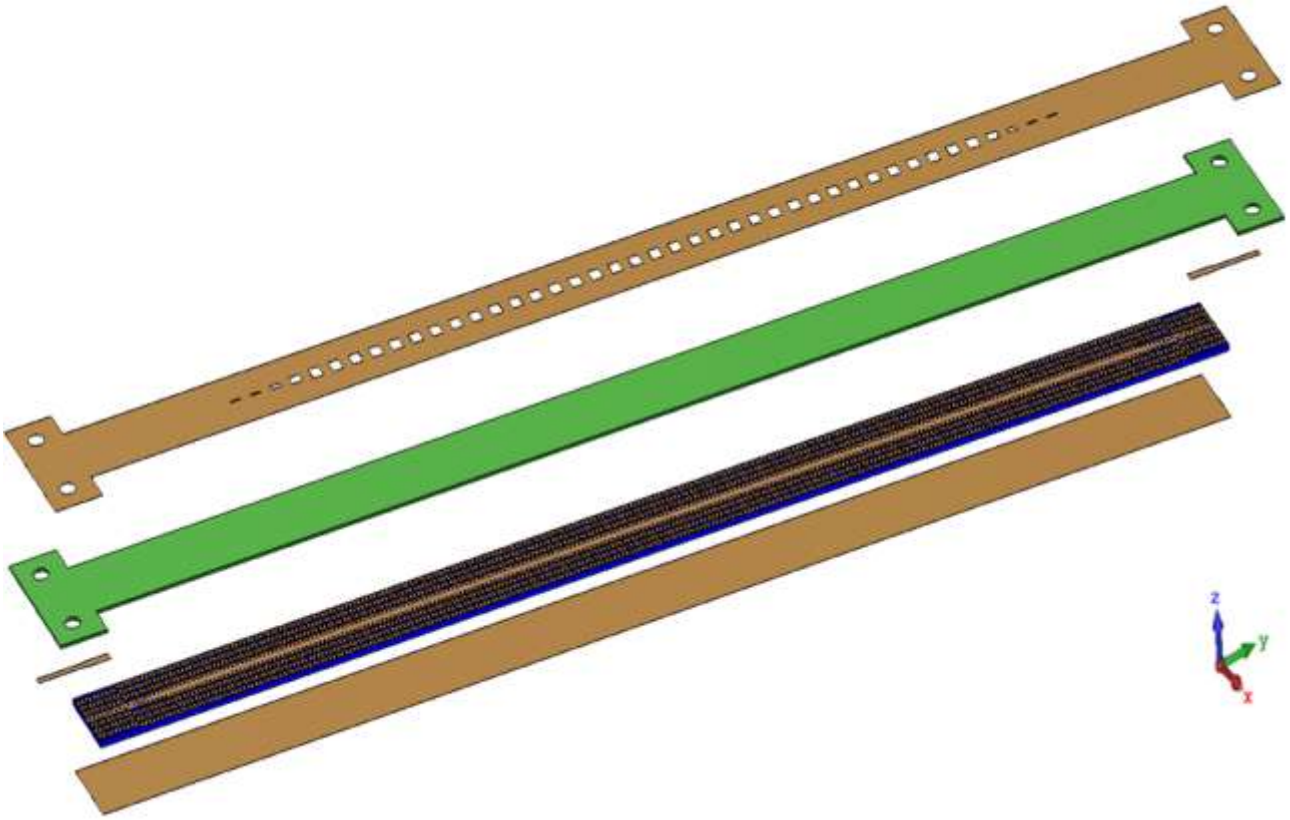

Figure. 3-13 (b). Configuration of layers for SIGW-LWA with MS line.

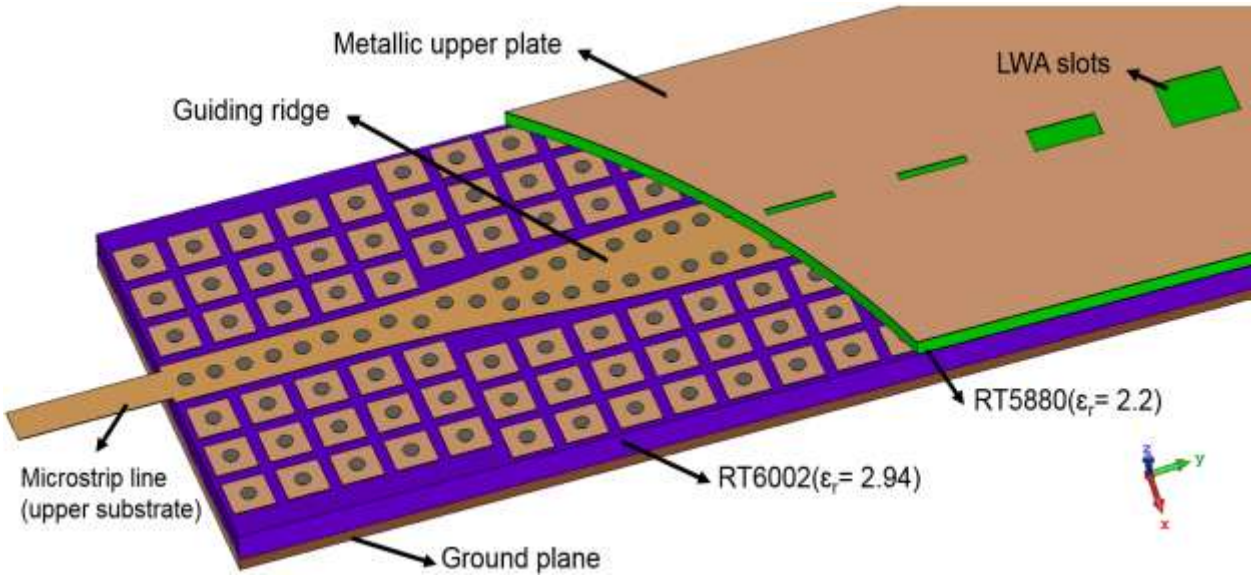

Figure. 3-13 (c). Close of to the MS transition with part of the upper substrate removed.

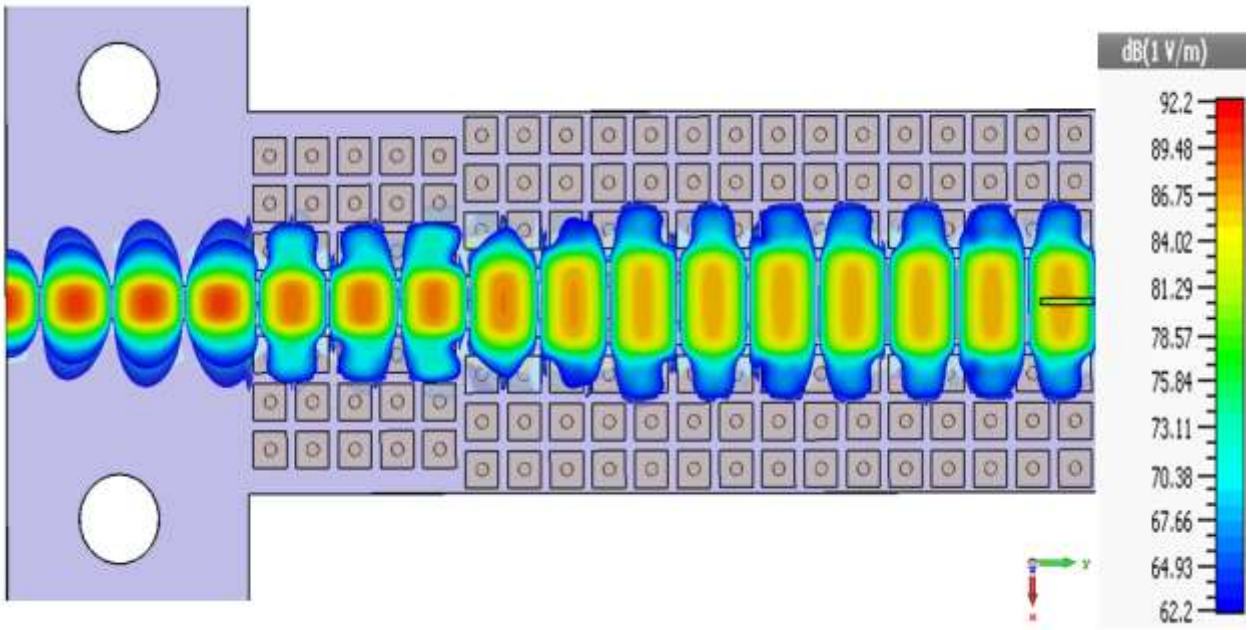

Figure. 3-14 Uniform field distribution for the SIGW-LWA for the structure of Figure.3-11 (f = 60 GHz).

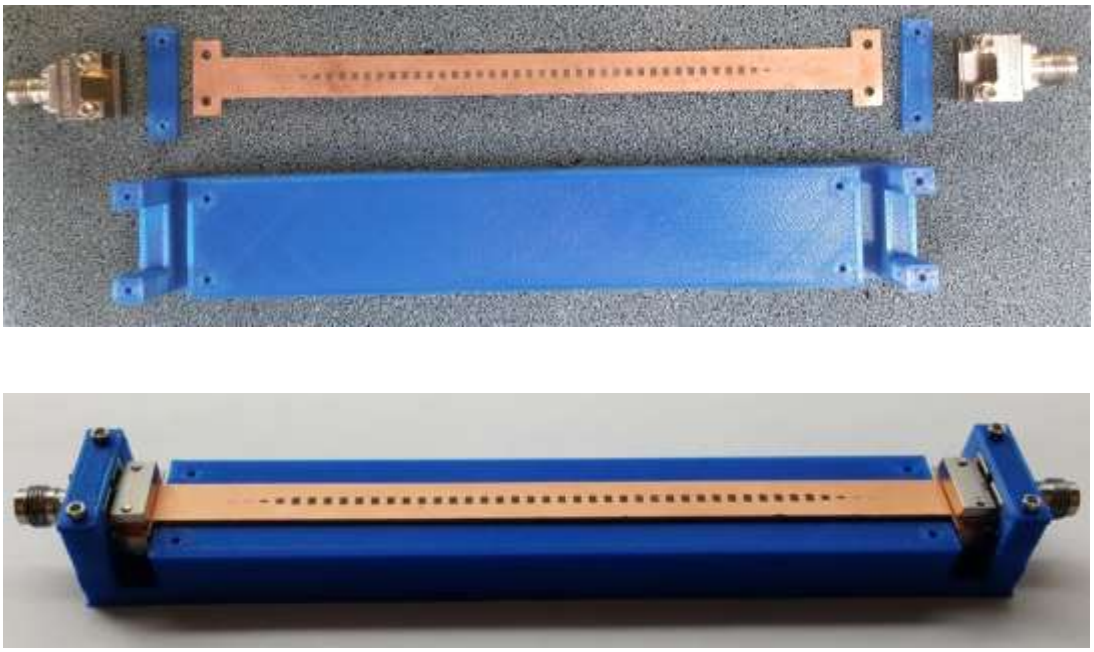

Figure. 3-15. Configuration fabricated prototype of SIGW-LWA.

3.5. Simulation and Measurement Results of SIGW-LWA

The simulated and measured *S*-parameters of the SIGW-LWA hold by the 3D-printed base is shown in Figure. 3-16. The reflection coefficients are below -15 dB with good agreement between simulated and measured results. Figure. 3-17 shows the measured and simulated leakage ratio of the proposed antenna. The antenna has a low and constant normalized leakage constant less than 0.02 $(\alpha/k_0 < 0.02)$ indicating that we have a narrow beam and long effective aperture. For this antenna, the phase and group velocity are in opposite directions and the phase constant is negative (β_{-1} < 0) in the frequency range of 57-64 GHz. The wave is physical backward proper fast wave and the power flows inward radially, based on LWA analysis given in [59], and [60]. Figure. 3-18 shows the realized gain of the co-polar E-plane radiation pattern for two frequencies at the first and the end of the desired bandwidth (57 GHz and 64 GHz). The measured peak gain of the antenna is 17.67 dBi with less than 1.3 dBi variation. The beam scanning range of the antenna is from –36 ° to –16 ° over the bandwidth. The cross-polar patterns for all frequencies in E-plane are below 30 dB from the main beam and they are not shown in Figure. 3-18. This LWA has a narrow fan beam radiation pattern due to the significant width of the antenna in the x-direction. Figure. 3-19 shows the 3D-radiation pattern of SIGW-LWA at 64 GHz. When the main beam is off the broadside direction (θ = 0°), H-plane pattern measurement is difficult, and the lab is not prepared for that. Therefore, we trust the simulated result, which shows good agreement with E-plane measurements. Figure. 3-20 shows the simulated H-plane at three different frequencies of the bandwidth for different θ angles.

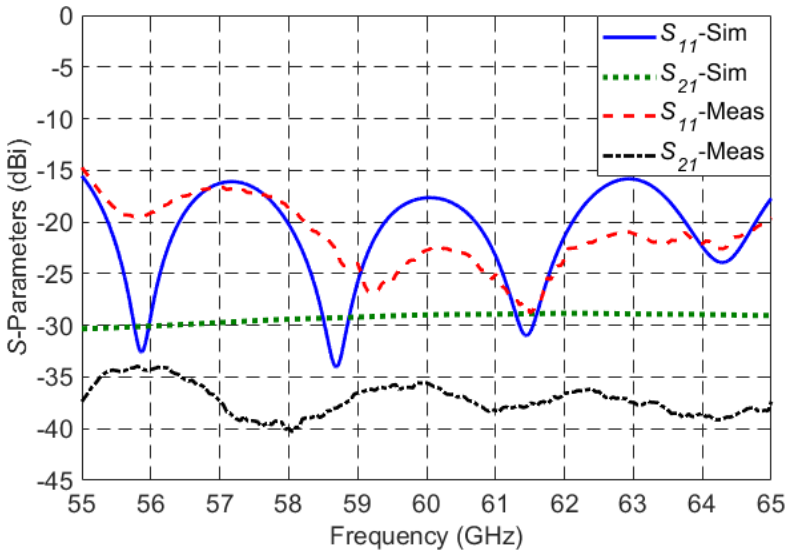

Figure. 3-16. Measured and simulated *S*-parameters of SIGW-LWA of structure in Figure.3-11.

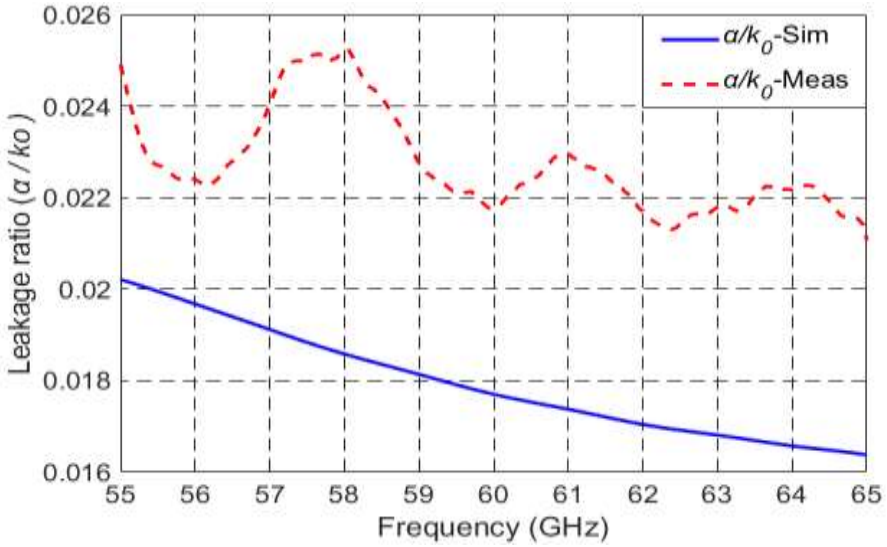

Figure. 3-17. Measured and simulated leakage ratio of SIGW-LWA of structure in Figure. 3-13.

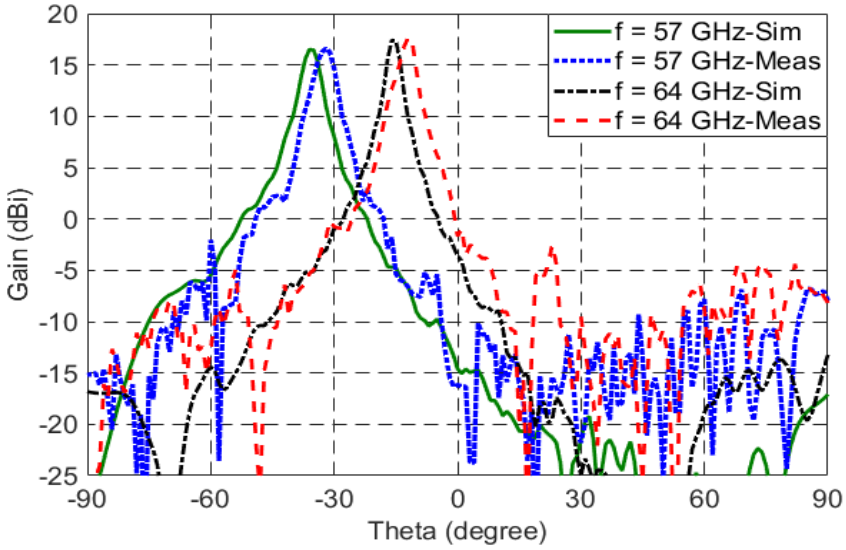

Figure. 3-18. Comparison between the measured and simulated realized gain of the co-polar E-plane radiation pattern for two different frequencies 57 GHz and 64 GHz.

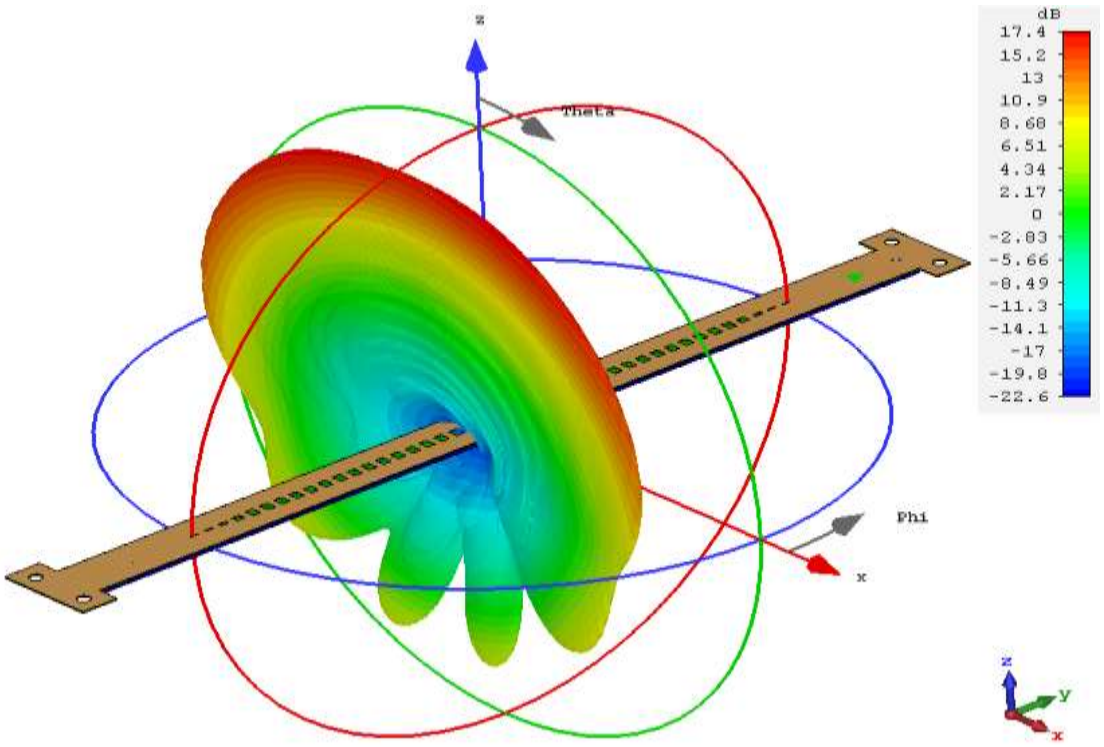

Figure. 3-19. Simulated 3D-Radiation pattern of SIGW-LWA at 64 GHz.

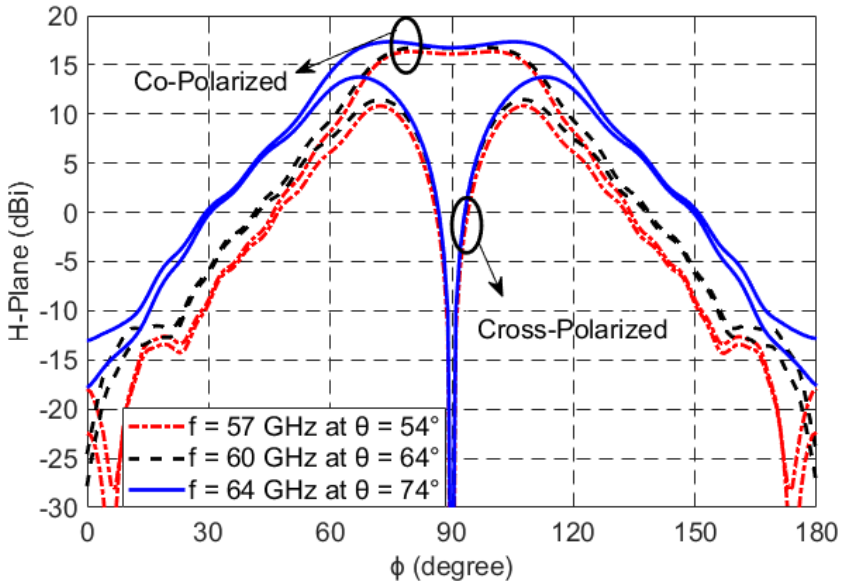

Figure. 3-20. The simulated co- and cross-polar H-plane radiation pattern at three frequencies, 57 GHz, 60 GHz and 64 GHz at θ=54°, θ=64°, and θ=74°, respectively for the antenna in Figure. 3-13.

3.6. Conclusion

A new design of LWA based on SIGW technology for millimeter-wave frequency band has been presented. The proposed antenna has achieved almost constant high gains, high radiation efficiency with wide impedance bandwidth at millimeter-wave frequencies. The antenna has been simply fabricated in a two-layered substrate and fed by a microstrip line. The bandwidth of the designed SIGW-LWA has achieved 29% around the center frequency of 58.5 GHz with a measured peak gain of 17.67 dBi with less than 1.3 dBi variation with more than 89% radiation efficiency over the frequency of 57-64 GHz. Good agreement between simulated and measured results of the SIGW-LWA design has been achieved. Compare to the SIW-LWA the proposed antenna has a higher radiation efficiency and higher gain with no sidelobe. In addition, compared to the RGW-LWA there is no need for the CNC machining which results in a low-cost fabrication process for the SIGW-LWA.

Chapter 4

Parallel Fed Two Elements Array

4.1. Introduction

In this chapter, we introduce a new design of a linear array of the LWA based on SIGW technology. One of the common problems of an array of the 1-D PLWA is that usually, this kind of antenna has a narrow bandwidth and considerable gain variation in their operating frequency band. To overcome these problems, first, a new wideband Y-shape power divider based on SIGW technology is designed. Secondly, a 1x2 array base of the presented SIGW-LWA in the previous chapter is also designed which can achieve a 3 dB gain increased and has a high radiation efficiency for all its operating frequency bands. The proposed antenna is designed to be fabricated on a two-layer substrate and fed by a transition from the microstrip to the SIGW.

4.2. Designing of a power divider based on Substrate-Integrated Printed Ridge Gap waveguide Technology

In the following section, a design of a two parallel SIGW-LWA is presented. In order to achieve this purpose, a power divider is designed to feed each SIGW-LWA element. A Y-shaped power divider is designed to cover the whole frequency range of the single SIGW-LWA, which is shown in Figure. 4-1. The same periodic structure used for the LWA design with the cell configuration given in Figure. 3-1 is used in this SIGW power dividing circuit. The upper substrate and metal top plate for the transition of the microstrip are not shown in Figure. 4-1. The SIGW power divider arms are designed to match with 50 Ω , and they are excited with the 50 Ω MS lines with the width of w_0 = 0.74 mm on the Rogers RT5880 substrate with ε_r = 2.2. Since the SIGW line and microstrip line have different propagation environments, the 50 Ω line of SIGW is achieved with the width of w_1 = 1 mm. A quarter-wavelength transformer with a characteristic impedance of 35.3 Ω is used to match the 50 Ω line with two arms of the Y-shaped power divider. The length and width of a quarter-wavelength transformer are L_2 = 1.9 mm, and w_2 = 1.52 mm, respectively. Figure. 4-2 shows the simulated *S*-parameters of the

power divider. The magnitude of S_{11} is below -15 dBi for all the operating frequency range. The insertion loss (|S_{21}|^2 + (|S_{31}|^2) of the Y shape power divider is 0.9.

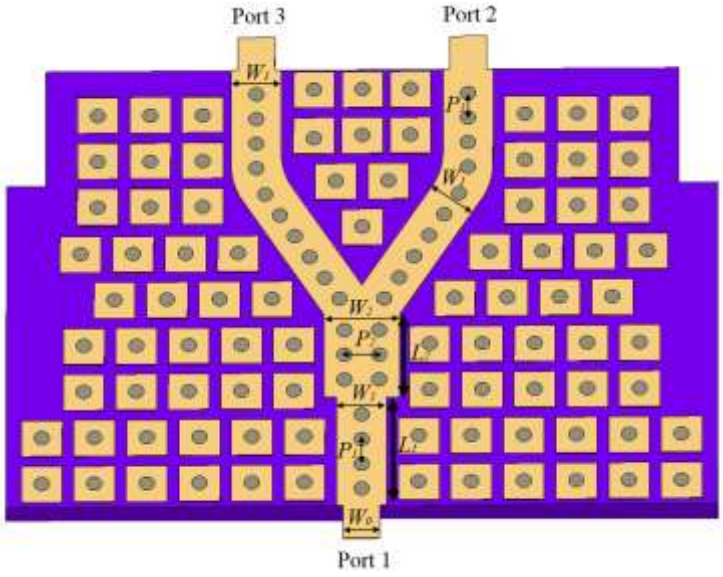

Figure. 4-1. Top view of a 1×2 SIGW Y-shape power divider (p_1 = 0.56 mm, p_2 = 0.89 mm, w_1 = 1 mm, w_2 = 1.52 mm, w_3 = 0.74 mm, L_1 = 2.46 mm, L_2 = 1.9 mm).

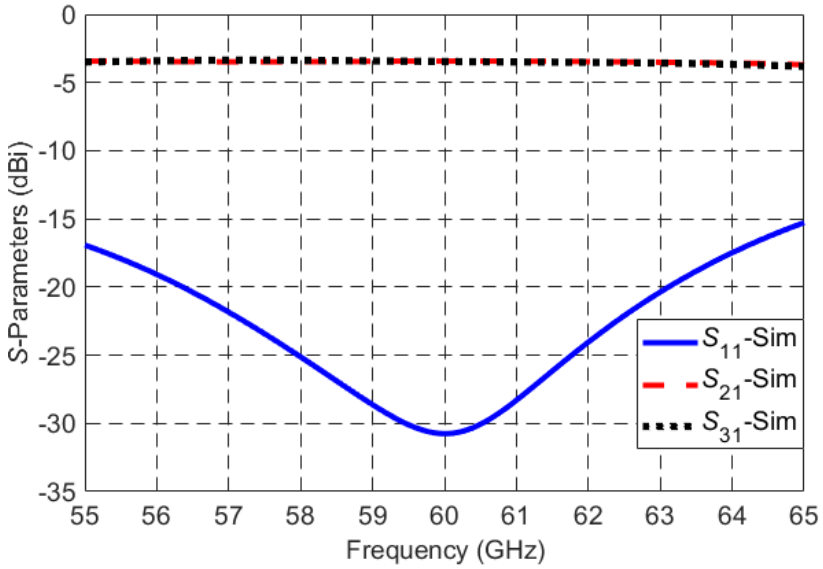

Figure. 4-2. Simulated *S*-parameters of the Y-shape power divider.

4.3. Array Design: Simulated and Measured Result

In order to avoid the appearance of grating lobes, the distance between the two subarrays is considered to be less than λ_0. Two arms of the Y-shape power divider is extended to connect LWA subarrays as shown in Figure. 4-3. In this design, the same power divider is used on the other side of the array to be able to connect the array to a single match load. Since the width of the SIGW ridgeline feeding the periodic slots is wider than 50 Ω line, after the power divider section of the array, two rows of periodic patches are placed between two ridgelines.

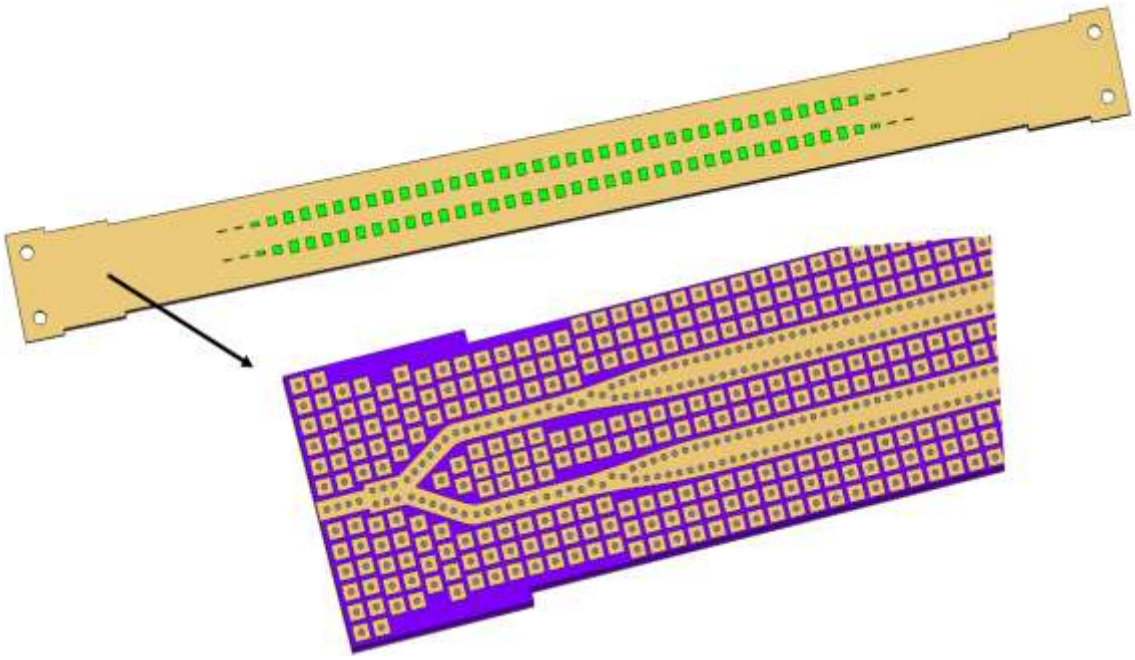

Figure 4-3. Configuration of an array of SIGW-LWA.

Simulated *S*-parameters of the proposed array are shown in Figure. 4-6. The reflection coefficient of the array is below -10 dBi for the entire operating frequency range. Such as single LWA, the array design also has a low and constant leakage ratio over the band proving the narrow beam radiation and long effective aperture. As the length of the antenna is long enough to radiate more than 90% of the power (total length = $34\lambda_0$), there is just a little power left at the end of the array. Therefore, instead of using another power divider for the matched load connection, two ends of each subarray are bent to connect together, as shown in Figure. 4-4. In this way, the weak propagation at the end of the each LWA sees the same characteristic impedance of SIGW.In other words, instead of using two matched loads at the end of each subarray, we use each Single array connected in series to act as a matched load for the other one. In addition, with this bending termination, the total length of the antenna is decreased

around $6\lambda_0$. Furthermore, the bend length is considered to be an odd multiple of a half wavelength. As such, the remaining power constructively contributes to the radiation. This design of the array is chosen for fabrication. Figure. 4-5 shows the configuration and fabricated prototype of the bend terminated array with the 3D-printed holder.

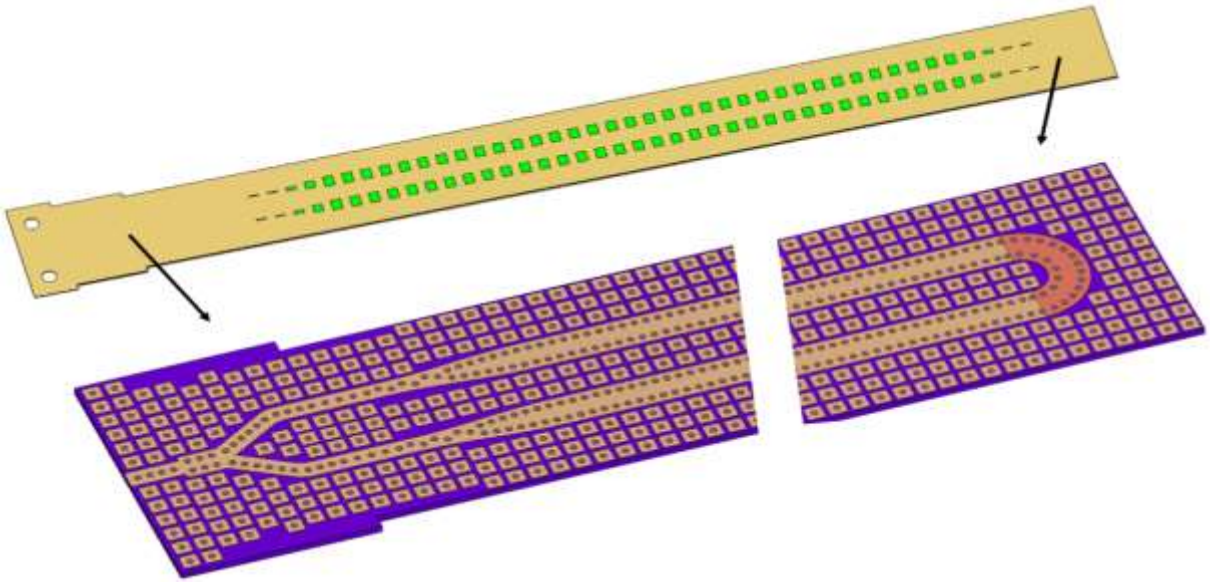

Figure. 4-4. Configuration of the bend terminated array of SIGW-LWA.

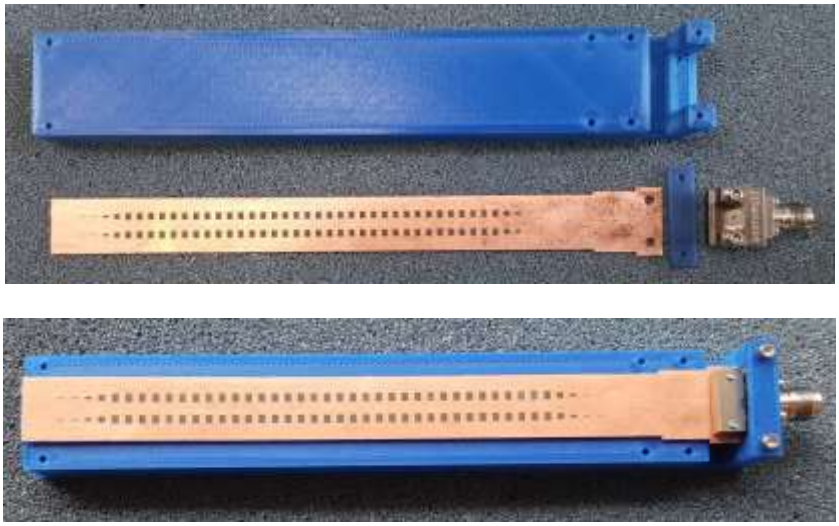

Figure. 4-5. Fabricated prototype of the bend terminated array of SIGW-LWA.

The simulated and measured *S*-parameters of the bend terminated array are shown in Figure. 4-6. The simulated reflection coefficients of bend terminated and matched load terminated arrays are the same and both of them are below -10 dB over the operating frequency band. There is good agreement between the simulated and measured results.

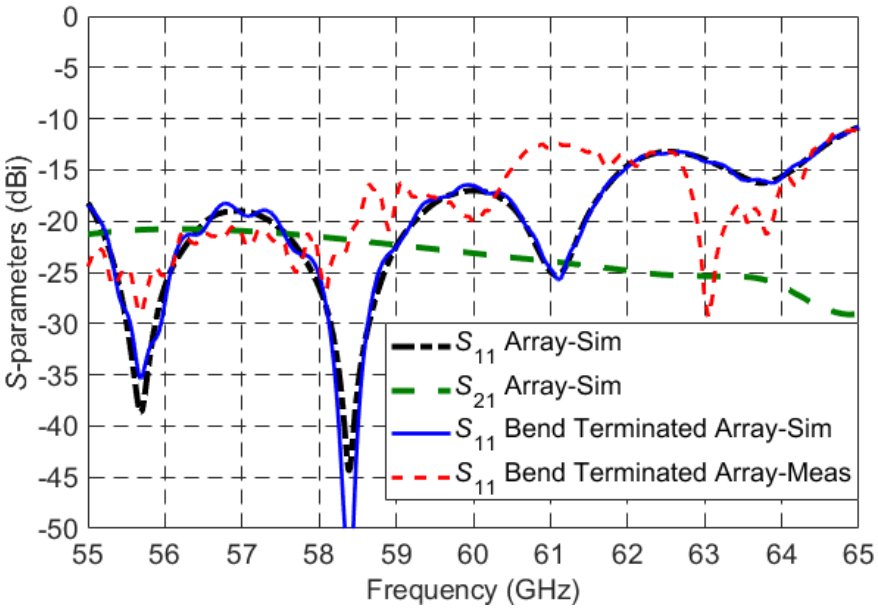

Figure. 4-6. Measured and simulated *S*-parameters of array and bend terminated array of SIGW-LWA of the structure of Figure. 4-3 and Figure. 4-4.

Figure. 4-7 shows the simulated and measured realized gain of the co-polar E-plane radiation pattern of the array and bend terminated array for two different frequencies 57GHz and 64GHz. Both array antennas can achieve a 3 dB gain increment due to the constructive coupling of the slots. In the bend terminated array, some minor lobes appear on the forward quadrant due to the weak power remaining at the end of each subarray. However, by considering the bend length as an odd multiple of half wavelength the level of the minor lobes in the forward quadrant decreases. For the proposed antenna the level of the minor lobes in the forward quadrant is 20 dB below the peak of the main beam for all the frequency bands. In addition, the level of the peak gain of the bend terminated array antenna is a little higher due to the constructive contribution of the remaining power to the radiation. The cross-polar E-plane patterns of all frequencies are below 27 dB from the main beam peak, and they are not shown in Figure. 4-7. There is a small discrepancy for the beam angle observed due to the shift of the frequency due to the length of the microstrip transition to SIGW. Figure. 4-8 shows the 3D-

radiation pattern of SIGW-LWA at 57 GHz. When the main beam is off the broadside direction (θ = 0°), H-plane pattern measurement is difficult and the lab is not prepared for that. Therefore, we trust the simulated result, which shows good agreement with E-plane measurements. Figure. 4-9 shows the simulated H-plane at three different frequencies of the bandwidth for different θ angles. Figure. 4-10 shows the realized gain with radiation efficiency and total efficiency for both array antennas and a single element of SIGW-LWA. The measured peak gain of the bend terminated array is 21.5 dBi with less than 1.3 dBi variation and -15 dB sidelobe level. The beam scanning range of the proposed array is from –35˚ to –15˚ in the frequency range of 57-64 GHz. The radiation efficiency for both array antennas is more than 87% over the operating frequency band. The total efficiency of the bend terminated array is more than 84%, which is a little higher than the simple array. Table. 1 shows a comparison between this work and others work of LWAs.

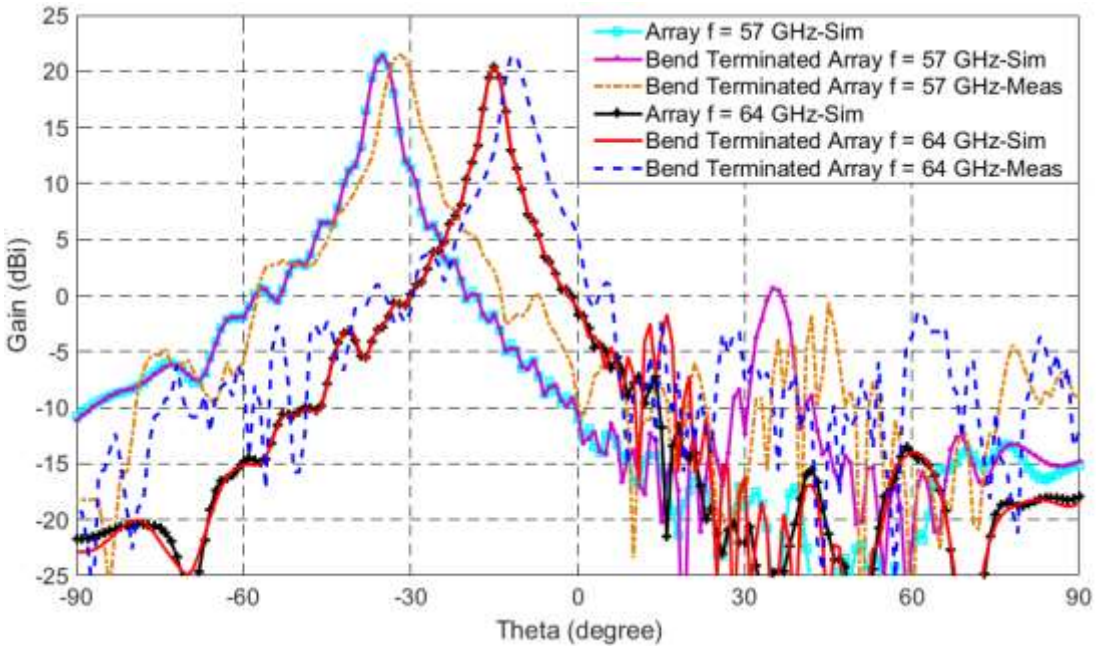

Figure. 4-7. Comparison between the measured and simulated realized gain of the co-polar E-plane radiation pattern for array and bend terminated array of SIGW-LWA for two different frequencies 57 GHz and 64 GHz.

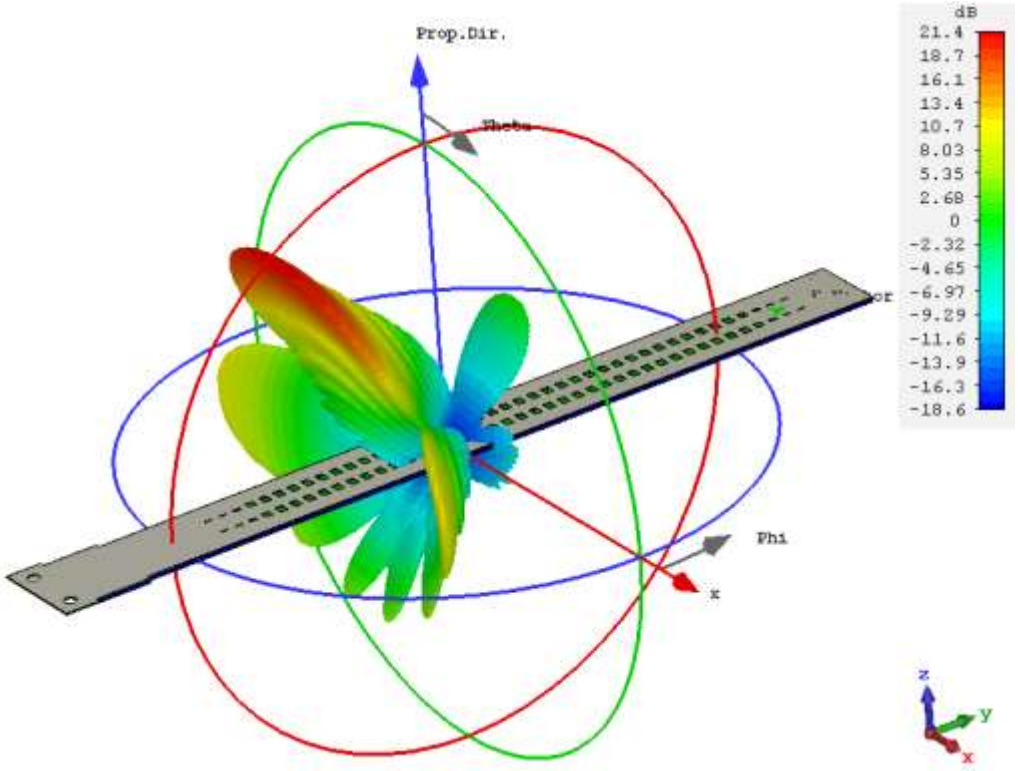

Figure. 4-8. Simulated 3D-Radiation pattern of SIGW-LWA at 57 GHz.

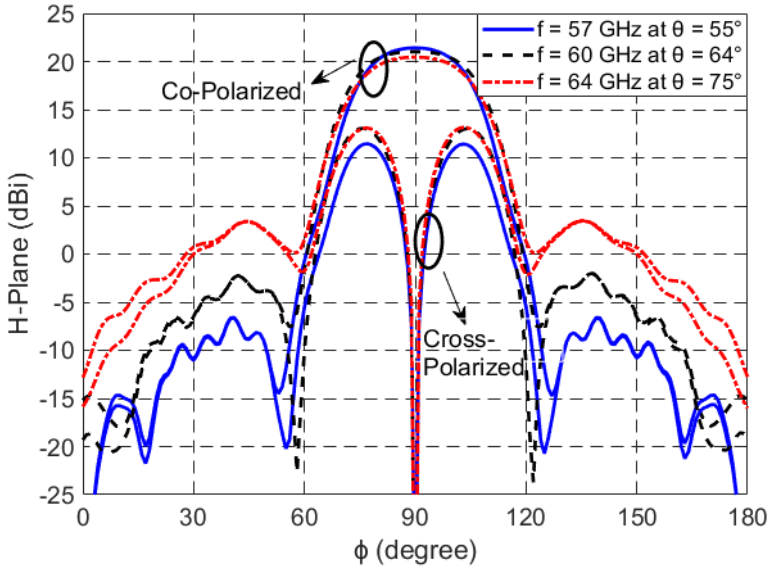

Figure. 4-9. The simulated co- and cross-polar H-plane radiation pattern at three frequencies, 57 GHz, 60 GHz and 64 GHz at θ = 54°, θ = 64°, and θ = 74°, respectively for the antenna in Figure. 4-4.

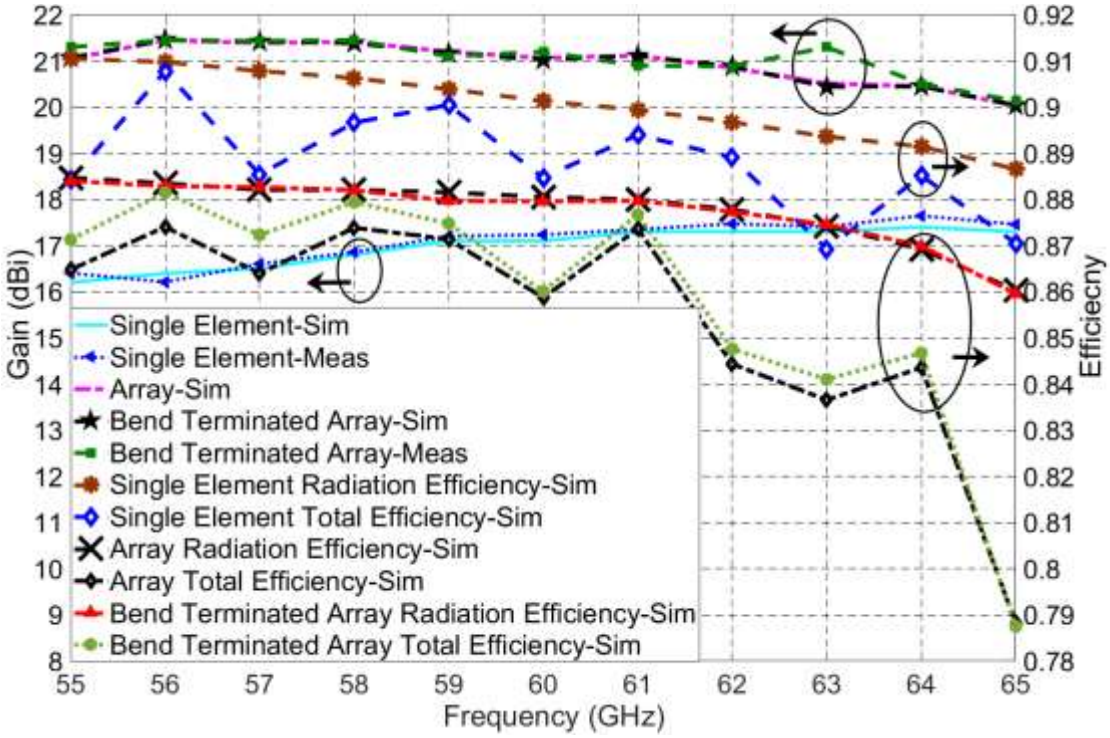

Figure. 4-10. Simulated and measured realized gain vs. Frequency for both array antennas and a single element of SIGW-LWA with simulated radiation efficiency and total efficiency.

Table. 1. The comparison of the proposed single element and bend terminated array of SIGW-LWA with the former LWAs.

Antenna	BW %	Gain (dBi)	Radiation Efficiency (%)	Length (λ_0)
Single Element (V-band) (This Work)	29	17.67	89	28
Bend Terminated Array (V-band) (This Work)	23	21.5	87	29
SIW-LWA (X-band) [47]	22	12	70	12
Butter Fly LWA (X-band) [50]	17	14.8	-	14
Quasi-Uniform LWA (X-band) [57]	16	14.8	-	10
SIW-MED-LWA (Ka-band) [68]	20	15.6	83	12
Dual-Beam DG-LWA (V-band) [69]	10	25 (F) 24 (B)	-	58
LWA-RGW feed by magic tee (K-band) [70]	14	15	-	15

4.4. Conclusion

A new design of a linear type of an array of LWA based on SIGW technology for millimeter-wave frequency (WiGig-band) band has been presented. The proposed array has achieved almost constant high gains, high radiation efficiency and wide impedance bandwidth at millimeter-wave frequencies. The proposed antenna has been fabricated in a two-layered substrate and fed by a microstrip line. The bandwidth of the designed array of the SIGW-LWA has achieved 23% around the center frequency of 59 GHz with a measured peak gain of 21.5 dBi with less than 1.3 dBi variation and -15 dB sidelobe level with more than 87% radiation efficiency over the frequency of 57-64 GHz. Good agreement between simulated and measured results of the SIGW-LWA design has been achieved. Compared to the SIW-LWA and CRLH-LWA, the proposed antenna has a higher radiation efficiency and almost a steady gain. In addition, compared to the RGW-LWA, there is no need for the CNC machining which results in a low-cost fabrication process for the SIGW-LWA.

Chapter 5. Conclusion and Future Work

The thesis has presented three novel designs of LWA using gap-waveguide technology. Gap waveguide technology is an air-filled guiding structure, which does not need any electrical contact between the layers, is very attractive for millimeter wave applications. The printed version of the RGW compared to the hollow waveguide and RGW, which have high fabrication cost, can be represented as a proper alternative for low-loss and low-cost guiding structures. However, ensuring a uniform thin air gap for PRGW structures at millimeter waves is problematic for large structures. Therefore, the gap is filled with a thin low-loss and low dielectric constant substrate layer to guarantee a fixed gap height for this guiding structure, which is referred to substrate integrated gap waveguide.

In Chapter 3, a novel design of 1-D PLWA based on the SIGW technology has been introduced. The antenna has been designed in order to excite the first space harmonic of the periodic structure as a leaky wave for the whole operation frequency band. The proposed antenna can be easily fed with a transition from microstrip to SIGW. In addition, it has an almost constant gain for the whole operation frequency band due to the constant leakage ratio. The proposed SIGW-LWA has better performance compared to the other LWAs such as a substrate integrated LWA, magnetoelectric dipole LWA and metamaterial based LWA in terms of the gain, radiation efficiency, and impedance bandwidth. In Chapter 4, a Y-shaped power divider and two linear arrays have been designed using the SIGW technology. The power divider has covered 30% of U-band and 44% of V-band. Both 1x2 array designs have achieved an almost constant gain with 3 dBi gain increment, and they have achieved a wide bandwidth same as the single element with low sidelobe level and a narrow beam due to the low constant leakage ratio of the antennas. In addition, for the two parallel fed arrays, a new termination has been considered, which resulted in a shorter physical length of the antenna. The objective of this thesis is to overcome the two common problems of LWAs in terms of gain variation and low radiation efficiency. In addition, all these three LWAs are designed for a WiGig application, which makes them more attractive for the 5G applications and today's industry requirements.

5.1. Future Work

Several other LWAs can be developed and designed based on the SIGW technology due to their characteristics as a low-loss, low-cost and high performance guiding structure for

millimeter-wave frequencies. According to the flexibility of the shape of the ridgeline of the SIGW, they can be used as a guiding structure for the 2-D PLWAs or slot array antennas in order to get a pencil beam type of radiation pattern. Furthermore, a dual-beam LWA based on the SIGW technology can be efficiently designed for WiGig application due to the excitation of the second space harmonic with first space harmonic simultaneously. In addition, a double SIGW can even be designed in order to achieve a high gain LWA with the multi-beam type of the radiation pattern. In conclusion, designing LWAs base on the printed version of the RGW could be more beneficial compared to the other technologies especially for the millimeter-wave applications due to their lower-losses and lower-cost. In addition, compared to the other designs of LWAs the performance of the SIGW-LWAs is better, which is the achieved goal of this thesis.

References

[1] S. Gong and M. Karlsson, "Pushing the wireless data rate to the internet speed," *IEEE Access*, vol. 4, pp. 8787-8792, 2016.

[2] E. K. MacHale, G. Talli, and P. D. Townsend, "10 Gb/s bidirectional transmission in a 116 km reach hybrid DWDM-TDM PON," *2006 Optical Fiber Communication Conference and the National Fiber Optic Engineers Conference,* 2006, pp. 3 pp.

[3] H. Mopidevi. et al.,"Three-dimensional microfabricated broadband patch antenna for WiGig applications," *IEEE Antennas Wireless Propag.Lett*, vol. 13, pp. 828-831, 2014.

[4] E. Pucci, A. U. Zaman, E. Rajo-Iglesias, P. S. Kildal and A. Kishk, "Losses in ridge gap waveguide compared with rectangular waveguides and microstrip transmission lines," *Proceedings of the Fourth European Conference on Antennas and Propagation*, Barcelona, Spain, 2010, pp. 1-4.

[5] A. Sain and K. L. Melde, "Impact of ground via placement in grounded coplanar waveguide interconnects," *IEEE Trans. Compon, Packag Technology*, vol. 6, no. 1, pp. 136-144, Jan. 2016.

[6] D. Deslandes and Ke Wu, "Accurate modeling, wave mechanisms, and design considerations of a substrate integrated waveguide," *IEEE Trans. Microw Theory Tech*, vol. 54, no. 6, pp. 2516-2526, June 2006.

[7] A. A. Brazalez, A. U. Zaman and P. S. Kildal, "Improved microstrip filters using PMC packaging by lid of nails," *IEEE Trans. Compon, Packag Technology*, vol. 2, no. 7, pp. 1075-1084, July 2012.

[8] M. P. Robinson *et al*., "Shielding effectiveness of a rectangular enclosure with a rectangular aperture," *Electronics Letters*, vol. 32, no. 17, pp. 1559-1560, 15 Aug 1996.

[9] M. Bozzi, M. Pasian, L. Perregrini and Ke Wu, "On the losses in substrate integrated waveguides," *2007 European Microwave Conference*, Munich, 2007, pp. 384-387.

[10] T. Ben Chaieb, A. Nasri, and H. Zairi, "Low loss substrate integrated waveguide slot antenna," *2017 International Conference on Advanced Systems and Electric Technologies (IC_ASET)*, Hammamet, 2017, pp. 25-29.

[11] A. Chen, A. J. B. Jasim Mousa, Y. Zhuang, Y. Huang and J. Zhou, "Compact Ka-band substrate-integrated waveguide filter with spurlines for satellite communication systems," *2016 IEEE 9th UK-Europe-China Workshop on Millimetre Waves and Terahertz Technologies (UCMMT)*, Qingdao, 2016, pp. 10-11.

[12] A. K. Ozturk and R. Paknys, "Analysis of propagation between rows of conducting cylinders that model solid surfaces using the same surface area rule," *IEEE Trans.Antennas Propag*, vol. 60, no. 5, pp. 2602-2606, May 2012.

[13] Feng Xu and Ke Wu, "Guided-wave and leakage characteristics of substrate integrated waveguide," *IEEE Trans. Microw Theory Tech*, vol. 53, no. 1, pp. 66-73, Jan. 2005.

[14] P. S. Kildal, "Definition of artificially soft and hard surfaces for electromagnetic waves," *Electronics Letters*, vol. 24, no. 3, pp. 168-170, 4 Feb 1988.

[15] E. Lier and P. S. Kildal, "Soft and hard horn antennas," *IEEE Trans.Antennas Propag*, vol. 36, no. 8, pp. 1152-1157, Aug. 1988.

[16] P. S. Kildal, "The hat feed: A dual-mode rear-radiating waveguide antenna having low cross polarization," *IEEE Trans.Antennas Propag*, vol. 35, no. 9, pp. 1010-1016, Sep 1987.

[17] P. S. Kildal and E. Lier, "Hard horns improve cluster feeds of satellite antennas," *Electronics Letters*, vol. 24, no. 8, pp. 491-492, 14 April 1988.

[18] M. N. M. Kehn and P. S. Kildal, "Miniaturized rectangular hard waveguides for use in multi frequency phased arrays," *IEEE Trans.Antennas Propag*, vol. 53, no. 1, pp. 100-109, Jan. 2005.

[19] A. Valero-Nogueira, E. Alfonso, J. I. Herranz and P. S. Kildal, "Experimental demonstration of local quasi-TEM gap modes in single-hard-wall waveguides," *IEEE Microw. Wireless Compon. Lett*, vol. 19, no. 9, pp. 536-538, Sept. 2009.

[20] P. S. Kildal, E. Alfonso, A. Valero-Nogueira, and E. Rajo-Iglesias,“Local metamaterial-based waveguides in gaps between parallel metal plates,” *IEEE Antennas Wireless Propag.Lett,* vol. 8, pp. 84–87, 2009.

[21] P. S. Kildal and M. N. M. Kehn, "The ridge gap waveguide as a wideband rectangular hard waveguide," *Proceedings of the Fourth European Conference on Antennas and Propagation*, Barcelona, Spain, 2010, pp. 1-4.

[22] A. Vosoogh, M. Sharifi Sorkherizi, A. Uz Zaman, J. Yang and A. A. Kishk, "An E-band antenna-diplexer compact integrated solution based on gap waveguide technology," *2017 International Symposium on Antennas and Propagation (ISAP)*, Phuket, 2017, pp. 1-2.

[23] E. A. Alós, A. U. Zaman and P. S. Kildal, "Ka-band gap waveguide coupled-resonator filter for radio link diplexer application," *IEEE Transactions on Components, Packaging and Manufacturing Technology*, vol. 3, no. 5, pp. 870-879, May 2013.

[24] M. Al Sharkawy, A. Foroozesh, A. A. Kishk and R. Paknys, "A robust horn ridge gap waveguide launcher for metal strip grating leaky wave antenna," *IEEE Trans.Antennas Propag*, vol. 62, no. 12, pp. 6019-6026, Dec. 2014.

[25] P. S. Kildal, "Three metamaterial-based gap waveguides between parallel metal plates for mm/submm waves," *2009 3rd European Conference on Antennas and Propagation*, Berlin, 2009, pp. 28-32.

[26] A. Farahbakhsh, D. Zarifi, and A. U. Zaman, "A mmwave wideband slot array antenna

based on ridge gap waveguide with 30% bandwidth," *IEEE Trans.Antennas Propag*, vol. 66, no. 2, pp. 1008-1013, Feb. 2018.

[27] A. Farahbakhsh, D. Zarifi, and A. U. Zaman, "60-GHz groove gap waveguide based wideband H-plane power dividers and transitions: For use in high-gain slot array antenna," *IEEE Trans. Microw Theory Tech*, vol. 65, no. 11, pp. 4111-4121, Nov. 2017.

[28] P. S. Kildal, A. U. Zaman, E. Rajo-Iglesias, E. Alfonso and A. Valero-Nogueira, "Design and experimental verification of ridge gap waveguide in bed of nails for parallel-plate mode suppression," *IET Microwaves, Antennas & Propagation*, vol. 5, no. 3, pp. 262-270, Feb. 21 2011.

[29] A. A. Brazález, E. Rajo-Iglesias, J. L. Vázquez-Roy, A. Vosoogh and P. S. Kildal, "Design and validation of microstrip gap waveguides and their transitions to rectangular waveguide, for millimeter-wave applications," *IEEE Trans. Microw Theory Tech*, vol. 63, no. 12, pp. 4035-4050, Dec. 2015.

[30] D. Zarifi, A. Farahbakhsh, A. U. Zaman and P. S. Kildal, "A high gain ridge gap waveguide fed slot antenna array for 60 GHz applications," *2016 10th European Conference on Antennas and Propagation (EuCAP)*, Davos, 2016, pp. 1-3.

[31] S. I. Shams and A. A. Kishk, "Printed texture with triangle flat pins for bandwidth enhancement of the ridge gap waveguide," *IEEE Trans. Microw Theory Tech*, vol. 65, no. 6, pp. 2093-2100, June 2017.

[32] E. Rajo-Iglesias and P. S. Kildal, "Numerical studies of bandwidth of parallel-plate cut-off realised by a bed of nails, corrugations and mushroom-type electromagnetic bandgap for use in gap waveguides," *IET Microwaves, Antennas & Propagation*, vol. 5, no. 3, pp. 282-289, Feb. 21 2011.

[32] M. M. M. Ali, S. I. Shams, and A. R. Sebak, "Printed ridge gap waveguide 3-dB coupler: analysis and design procedure," *IEEE Access*, vol. 6, pp. 8501-8509, 2018.

[33] M. Sharifi Sorkherizi, A. Dadgarpour, and A. A. Kishk, "Planar high-efficiency antenna array using new printed ridge gap waveguide technology," *IEEE Trans.Antennas Propag*, vol. 65, no. 7, pp. 3772-3776, July 2017.

[34] N. Bayat-Makou and A. A. Kishk, "Millimeter-wave substrate integrated dual level gap waveguide horn antenna," *IEEE Trans.Antennas Propag*, vol. 65, no. 12, pp. 6847-6855, Dec. 2017.

[35] M. Sharifi Sorkherizi and A. A. Kishk, "Fully printed gap waveguide with facilitated design properties," *IEEE Microw. Wireless Compon. Lett*, vol. 26, no. 9, pp. 657-659, Sept. 2016.

[36] C. H. Walter, "*Traveling Wave Antennas*," McGraw-Hill, New York, 1965.

[37] W. W. Hansen,"*Radiating electromagnetic waveguide*," U.S. Patent No. 2,402,622,

1940.

[38] [Bakhtiar Khan]. (2017, November 6). Public scholar program Bakhtiar Ali Khan. retrieved from http://www.easybib.com/guides/citation-guides/apa-format/youtube-video/

[39] T. Tamir, "Leaky-wave antennas, in *Antenna Theory*," *Part 2* , R. E. Collin and F. J. Zucker (Eds.), McGraw-Hill, New York, 1969, Chap. 20.

[40] A. Hessel, "General characteristics of traveling-wave antennas, in *Antenna Theory*," *Part 2*, R. E. Collin and F. J. Zucker (Eds.), McGraw-Hill, New York, 1969, Chap. 19.

[41] F. Sadjadi, M. Helgeson, M. Radke and G. Stein, "Radar synthetic vision system for adverse weather aircraft landing," *IEEE Trans.Aerosp.Electron.Syst*, vol. 35, no. 1, pp. 2-14, Jan 1999.

[42] S. Gu, C. Li, X. Gao, Z. Sun and G. Fang, "Terahertz aperture synthesized imaging with fan-beam scanning for personnel screening," *IEEE Trans. Microw Theory Tech*, vol. 60, no. 12, pp. 3877-3885, Dec. 2012.

[43] Young-Jin Park and W. Wiesbeck, "Offset cylindrical reflector antenna fed by a parallel-plate Luneburg lens for automotive radar applications in millimeter-wave," *IEEE Trans.Antennas Propag*, vol. 51, no. 9, pp. 2481-2483, Sep 2003.

[44] Y. Dong and T. Itoh, "Composite right/left-handed substrate integrated waveguide and half mode substrate integrated waveguide leaky-wave structures," *IEEE Trans.Antennas Propag*, vol. 59, no. 3, pp. 767-775, March 2011.

[45] Nasimuddin, Z. N. Chen and X. Qing, "Multilayered composite right/left-handed leaky-wave antenna with consistent gain," *IEEE Trans.Antennas Propag*, vol. 60, no. 11, pp. 5056-5062, Nov. 2012.

[46] W. Cao, Z. N. Chen, W. Hong, B. Zhang and A. Liu, "A beam scanning leaky-wave slot antenna with enhanced scanning angle range and flat gain characteristic using composite phase-shifting transmission line," *IEEE Trans.Antennas Propag*, vol. 62, no. 11, pp. 5871-5875, Nov. 2014.

[47] J. Liu, D. R. Jackson, and Y. Long, "Substrate integrated waveguide (SIW) leaky-wave antenna with transverse slots," *IEEE Trans.Antennas Propag*, vol. 60, no. 1, pp. 20-29, Jan. 2012.

[48] N. Yan, K. Ma, H. Zhang, and Z. Jian, "A novel substrate integrated suspended line wideband leaky-wave antenna," *IEEE Antennas Wireless Propag.Lett*, vol. 16, pp. 2642-2645, 2017.

[49] N. Nasimuddin, Z. N. Chen and X. Qing, "Substrate integrated metamaterial single-substrate integration technique of planar circuits and w-Based Leaky-Wave Antenna With Improved Boresight Radiation Bandwidth," *IEEE Trans.Antennas Propag*, vol. 61, no. 7, pp. 3451-3457, July 2013.

[50] Y. Mohtashami and J. Rashed-Mohassel, "A butterfly substrate integrated waveguide leaky-wave antenna," *IEEE Trans.Antennas Propag*, vol. 62, no. 6, pp. 3384-3388, June 2014.

[51] L. O. Goldstone and A. A. Oliner, "Leaky-wave antennas—Part I: Rectangular waveguides," *IRE Trans. Antennas Propag.*, Vol. 7, pp. 307–319, October 1959.

[52] Wanjing Huang, Wuqiong Luo, Bo Chen and Pu Tang, "A ferrite leaky-wave beam scanning antenna based on NRD waveguide," *2015 IEEE International Conference on Communication Problem-Solving (ICCP)*, Guilin, 2015, pp. 350-352.

[53] R. Gilbert, "Slot antenna arrays, in *Antenna Engineering Handbook*," 4th ed., J. L. Volakis (Ed.), McGraw-Hill, New York, 2007, Chap. 9.

[54] W. Croswell and F. J. Zucker, Surface-wave antennas, in *Antenna Engineering Handbook*, 4th ed., J. L. Volakis (Ed.), McGraw-Hill, New York, 2007, Chap. 10.

[55] A. B. Yakovlev, M. G. Silveirinha, O. Luukkonen, C. R. Simovski, I. S. Nefedov and S. A. Tretyakov, "Characterization of surface-wave and leaky-wave propagation on wire-medium slabs and mushroom structures based on local and nonlocal homogenization models," *IEEE Trans. Microw Theory Tech*, vol. 57, no. 11, pp. 2700-2714, Nov. 2009.

[56] P. Baccarelli, C. Di Nallo, S. Paulotto and D. R. Jackson, "A full-wave numerical approach for modal analysis of 1-D periodic microstrip structures," *IEEE Trans. Microw Theory Tech*, vol. 54, no. 4, pp. 1350-1362, June 2006.

[57] N. Javanbakht, M. S. Majedi, and A. R. Attari, "Thinned Array Inspired Quasi-Uniform Leaky-Wave Antenna With Low Side-Lobe Level," *IEEE Antennas Wireless Propag.Lett*, vol. 16, pp. 2992-2995, 2017.

[58] D. R. Jackson, C. Caloz and T. Itoh, "Leaky-Wave Antennas," *Proceedings of the IEEE*, vol. 100, no. 7, pp. 2194-2206, July 2012.

[59] C. A. Balanis, "Leaky-Wave Antennas," *Modern Antenna Handbook*, 1, Wiley Telecom, Chapter7, pp.338.

[60] R. Paknys, "Green Function Construction II," *Applied Frequency-Domain Electromagnetics*, Wiley, 2016, Chapter 12, pp.403.

[61] S. Paulotto, P. Baccarelli, F. Frezza and D. R. Jackson, "Full-Wave modal dispersion analysis and broadside optimization for a class of microstrip CRLH leaky-wave antennas," *IEEE Trans. Microw Theory Tech*, vol. 56, no. 12, pp. 2826-2837, Dec. 2008.

[62] S. Paulotto, P. Baccarelli, F. Frezza and D. R. Jackson, "Full-wave modal dispersion analysis and broadside optimization for a class of microstrip CRLH leaky-wave antennas," *IEEE Trans. Microw Theory Tech*, vol. 56, no. 12, pp. 2826-2837, Dec.

2008.

[63] P. Burghignoli, G. Lovat, and D. R. Jackson, "Analysis and optimization of leaky-wave radiation at broadside from a class of 1-D periodic structures," *IEEE Trans.Antennas Propag*, vol. 54, no. 9, pp. 2593-2604, Sept. 2006.

[64] C. Caloz, T. Itoh and A. Rennings, "CRLH metamaterial leaky-wave and resonant antennas," *IEEE Antennas and Propagation Magazine*, vol. 50, no. 5, pp. 25-39, Oct. 2008.

[65] R. C. Johnson (Ed.), Antenna Engineering Handbook, Third Edition, New York, McGraw Hill, 1992, Chapter 10.

[66] M. Sharifi Sorkherizi, A. Dadgarpour, and A. A. Kishk, "Planar high-efficiency antenna array using new printed ridge gap waveguide technology," *IEEE Trans.Antennas Propag*,, vol. 65, no. 7, pp. 3772-3776, July 2017.

[67] M. Sharifi Sorkherizi and A. A. Kishk, "Self-packaged, low-loss, planar bandpass filters for millimeter-wave application based on printed gap waveguide technology," *IEEE Transactions on Components, Packaging and Manufacturing Technology*, vol. 7, no. 9, pp. 1419-1431, Sept. 2017.

[68] K. M. Mak, K. K. So, H. W. Lai and K. M. Luk, "A magnetoelectric dipole leaky-wave antenna for millimeter-wave application," *IEEE Trans.Antennas Propag*, vol. 65, no. 12, pp. 6395-6402, Dec. 2017.

[69] Z. L. Ma, K. B. Ng, C. H. Chan and L. J. Jiang, "A novel supercell-based dielectric grating dual-beam leaky-wave antenna for 60-GHz applications," *IEEE Trans.Antennas Propag*, vol. 64, no. 12, pp. 5521-5526, Dec. 2016.

[70] S. I. Shams, M. A. Abdelaal, and A. A. Kishk, "Broadside uniform leaky-wave slot array fed by ridge gap splitted line," *2015 IEEE International Symposium on Antennas and Propagation & USNC/URSI National Radio Science Meeting*, Vancouver, BC, 2015, pp. 2467-2468.